SIMULATION AND ANALYSIS OF A TIME HOPPING SPREAD SPECTRUM COMMUNICATION SYSTEM

by

Jeffrey B. Mendola

Thesis submitted to the Faculty of the

Virginia Polytechnic Institute and State University

in partial fulfillment of the requirements for the degree of

MASTER OF SCIENCE

in

Electrical Engineering

APPROVED:

Brian D. Woerner, Chairman

Charles W. Bostian

Ivan Howitt

June 12, 1996

Blacksburg, Virginia

Keywords: Spread-Spectrum, Time-Hopping, Ultra-wideband, Multiple Access Communications, Gaussian approximation

LD
5655
V855
1996
M463
c.2

SIMULATION AND ANALYSIS OF A TIME HOPPING SPREAD SPECTRUM COMMUNICATION SYSTEM

by

Jeffrey B. Mendola

Thesis submitted to the Faculty of the

Virginia Polytechnic Institute and State University

in partial fulfillment of the requirements for the degree of

MASTER OF SCIENCE

in

Electrical Engineering

APPROVED:

Brian D. Woerner, Chairman

Charles W. Bostian

Ivan Howitt

June 12, 1996

Blacksburg, Virginia

Keywords: Spread-Spectrum, Time-Hopping, Ultra-wideband, Multiple Access Communications, Gaussian approximation

SIMULATION AND ANALYSIS OF A TIME HOPPING SPREAD SPECTRUM COMMUNICATION SYSTEM

by

Jeffrey B. Mendola

Brian D. Woerner. Chairman

Electrical Engineering

(ABSTRACT)

Lately, spread spectrum systems are being increasingly used for commercial wireless communications because of their ability to reject various types of interference. This ability allows them to be used in multiple access systems. Direct sequence and frequency hopping systems have been the primary spread spectrum techniques used in practice. One technique which has not received much attention until recently is time hopping. In time hopping, a symbol is transmitted at a random position within the symbol period using a pulse width which is much smaller than the symbol period. Ultra-wideband (UWB) technology is a radar technology which shows promise for an relatively simple implementation of a time hopping system.

This thesis looks at the error probability performance of a UWB time hopping multiple access system. Previous work has led to an estimate of the performance using a Gaussian approximation similar to that used for direct sequence systems. Through the use of a fast simulation technique, it will be shown that in certain situations, the Gaussian approximation fails to accurately predict the performance. A numerical analysis which uses characteristic functions is developed and shown to correctly predict the system's performance under a wide range of situations. This numerical analysis also contributes to the understanding of the system.

Acknowledgments

I would like to thank my advisor Dr. Brian Woerner for his help and advise throughout the research for and preparation of this thesis. I would also like to thank Dr. Ivan Howitt and Dr. Charles Bostian for their comments on my thesis.

My thanks also go to Robert James for the opportunity to work for the Center for Transportation Research and to be involved in interesting research.

Finally, I would like to thank my family for their support and encouragement throughout my studies.

Table of Contents

1. Introduction 1
1.1. Wireless Spread Spectrum Systems 1
1.2. UWB Time Hopping 2
1.3. Previous Work 5
1.4. Purpose of Thesis 6
1.5. Organization of Thesis 6
2. The UWB PPM Time Hopping System 8
2.1. Structure of the Transmitter 8
2.2. Channel Model 11
2.3. Structure of the Receiver 12
2.4. Summary 16
3. The Gaussian Approximation 18
3.1. Using the Gaussian Approximation for the UWB Time Hopping System 18
3.2. Determining the Mean and Variance of n_t 19
3.3. Calculating the Probability of Error 21
3.4. Summary 25
4. Simulation of the UWB PPM Time Hopping System 26
4.1. Purpose of the Simulation 26
4.2. Simulation Method 26
4.3. Simulation Implementation 29
4.4. Simulation Results 30
4.5. Summary of Results 38
5. A Numerical Analysis of the UWB PPM Time Hopping System 39
5.1. Purpose of the Analysis 39
5.2. Analysis Method 39
5.3. Modeling the Characteristic Function of R 41
5.4. Computing the Characteristic Function of the Total Receiver Noise 43
5.5. Computing the Probability of Error Using Characteristic Functions 44
5.6. Comparing the Numerical Analysis with the Simulation Results 45
5.7. Summary of Results 49
6. Discussion of Results 53
6.1. Insight Gained From the Numerical Analysis 53
6.2. A Look at the Convergence of the Gaussian Approximation 53
6.3. Significance of Important Performance Results 60
7. Conclusion 63
7.1. Summary of Thesis Results 63
7.2. Future Work 64
8. References 65
Vita 67

List of Figures

Figure 2.1 - A plot of $p(t)$ vs. t/τ_m 9
Figure 2.2 - Spectrum of the monocycle, $p(t)$, when the pulse width is 1 ns 10
Figure 2.3 - Transmitter Block Diagram 11
Figure 2.4 - A plot of $w(t)$ vs. t/τ_m 13
Figure 2.5 - Spectrum of $w(t)$ when the pulse width is 1 ns 14
Figure 2.6 - A plot of $v(t)$ vs. t/τ_m with δ/τ_m=0.5 15
Figure 2.7 - Spectrum of $v(t)$ when the monocycle pulse width is 1 ns and δ/τ_m=0.5 16
Figure 2.8 - Receiver Block Diagram 17
Figure 3.1 - Plot of $R_{wv}(t)/E_w$ vs. t/τ_m for δ=0.5τ_m 21
Figure 3.2. - Plot of P_e vs. E_b/N_o for different values of N_u with N=100 24
Figure 4.1 - Block diagram for the simulation approach 28
Figure 4.2 - Plot of P_e vs. E_b/N_o for different values of N_u with N_b=6 and T_f=80 31
Figure 4.3 - Plot of P_e vs. E_b/N_o for different values of N_b with N_u=6 and N_bT_f=480 32
Figure 4.4 - Plot of P_e vs. E_b/N_o for different values of N_b with N_u=6 and N_bT_f=480 33
Figure 4.5 - Plot of P_e vs. E_b/N_o for different values of N_b with N_u=11 and N_bT_f=960 34
Figure 4.6 - Plot of P_e vs. E_b/N_o for different values of N_b with N_u=11 and N_bT_f=960 35
Figure 4.7 - Plot of P_e vs. N_u for different values of T_f with N_b=1 and E_b/N_o=20 dB 36
Figure 4.8 - Plot of P_e vs. P_k/P_1 for different values of N_b with N_u=6, N_bT_f=480, and E_b/N_o=20 dB 37
Figure 5.1 - Plot of the cumulative distribution function of $R_{wv}(\tau)/E_w$ 40
Figure 5.2 - Plot of the linear spline approximation to $F_R(R)$ 42
Figure 5.3 -Plot of P_e vs. E_b/N_o for different values of N_u with N_b=6 and T_f=80 46
Figure 5.4 - Plot of P_e vs. E_b/N_o for different values of N_b with N_u=6 and N_bT_f=480 47
Figure 5.5 - Plot of P_e vs. E_b/N_o for different values of N_b with N_u=11 and N_bT_f=960 48
Figure 5.6 - Plot of P_e vs. E_b/N_o for different values of N_b with N_u=6 and N_bT_f=480 49
Figure 5.7 - Plot of P_e vs. E_b/N_o for different values of N_b with N_u=11 and N_bT_f=960 50
Figure 5.8 - Plot of P_e vs. N_u for different values of T_f with N_b=1 and E_b/N_o=20 dB 51
Figure 5.9 - Plot of P_e vs. P_k/P_1 for different values of N_b with N_u=6, N_bT_f=480, and E_b/N_o=20 dB 52
Figure 6.1 - Plot of P_e vs. N_u for different values of T_f with N_b=1 and E_b/N_o=20 dB 56
Figure 6.2 - Plot of P_e vs. N_b for different values of T_f with N_u=15 and E_b/N_o=12 dB 57
Figure 6.3 - Plot of P_e vs. N_b for different values of N_bT_f with N_u=15 and E_b/N_o=20 dB 58

List of Tables

Table 3.1 - Values of E_w/m_p and E_R / m_p^2 for various values of δ/τ_m.....23
Table 5.1 - Values of R_i used for the linear spline approximation to $F_R(R)$.....41
Table 5.2 - Values used for a_i and t_i.....43

1. Introduction

1.1. Wireless Spread Spectrum Systems

There has been a surge of interest in spread spectrum communications, especially for non-military applications. Military systems use spread spectrum for covert communications and their resistance to jamming. On the other hand, cellular phone networks and other wireless radio applications benefit from using spread spectrum systems because of their interference rejection capabilities. This interference rejection provides resistance to multipath fading. It also helps to reject narrowband interference which can allow these systems to be overlaid over existing narrowband channels. Most importantly, spread spectrum signals can reject other users' signals and this allows them to be used in a Code Division Multiple Access (CDMA) system. CDMA systems have the interesting property that the system performance degrades gracefully with increases in the number of users.

Currently, the two spread spectrum methods which are used in practice are direct sequence (DS) and frequency hopping (FH). In direct sequence, the binary data is multiplied by a binary, pseudo-random spreading sequence whose symbol rate is much higher than the data rate. Correlation with the pseudo-random spreading sequence provides the interference rejection. Right now, DS spread spectrum is the method which is used most often in practice. Currently, it is used in the IS-95 cellular radio standard, in unlicensed "Part 15" devices like cordless telephones, and in the Global Positioning System (GPS) which is a satellite positioning system.

In frequency hopping, the center frequency of the transmitter is changed in a pseudo-random manner. Interference rejection is obtained when the interference is narrowband because the transmitter will not always be transmitting on the frequency that the interference occupies. A slow frequency hopping system has a hopping rate (the rate at which the center frequency changes) which is slower than the data rate, and a fast frequency hopping system has a hopping rate which is faster than the data rate. Fast

frequency hopping provides diversity since each data bit is transmitted more than once, but it demands very stringent synchronization requirements. For this reason, most of today's systems use slow frequency hopping. Frequency hopping is employed in the GSM cellular radio standard to provide immunity to fading, and it is also used in Cellular Digital Packet Data (CDPD).

One method which until recently has received very little attention is called time hopping (TH). As one might guess, time hopping can be thought of as a dual of the frequency hopping method. In frequency hopping, the total transmission bandwidth is divided into many smaller channels, and then each user regularly switches which channel it uses in a pseudo-random manner. In time hopping, the bit period is divided into small time intervals with each user regularly switching the interval it uses in a pseudo-random manner. On the other hand, time hopping can also be thought of as a low duty cycle, time-varying version of direct sequence spread spectrum. The bandwidth spreading, which is common to all spread spectrum signals, is achieved by having each user only transmit for a small fraction of the bit period.

1.2. UWB Time Hopping

Time hopping has received little attention until recently. This because it has more stringent timing requirements than DS or FH and because in general the receiver is more complex than for the other methods. However, some recent developments have led to a technology which shows promise for relatively simple and low cost implementation of a time hopping system. This technology which is known as ultra-wideband technology and has grown out of the radar field. Ultra-wideband (UWB) technology was developed for radars for the purpose of getting fine resolution on range measurements. UWB technology basically uses signals with such large bandwidths that they can no longer be considered as conventional RF signals. These signals are characterized by their bandwidth to center frequency ratios. Narrowband systems have ratios less than 0.01, and conventional

wideband systems (such as other spread spectrum systems) will have ratios which are usually less than 0.25. UWB signals, however, have ratios in the range of 0.25 to 2.0. In a sense, these signals are really just baseband pulses of electromagnetic energy. Because of this, UWB technology is sometimes known as non-sinusoidal or impulse technology.

As can be seen, UWB signals are very different from the conventional signals normally used in communication systems. This fact has lead to some obstacles in the development of practical UWB systems. One obvious challenge is to develop transmitter circuitry which is able to transmit short duration pulses. However, there are currently devices being developed by a few companies which have sufficiently short pulses. Prototypes with pulses on the order of nanoseconds have been developed and tested. Another challenge in implementing UWB devices is developing devices which can transmit high powers. This is especially the case when the device is to be used in a long range radar system. Because UWB signals have low duty cycles, the devices must be able to handle much higher peak powers than those normal seen in conventional systems. The antenna used in an UWB system must also receive special attention. Since UWB signals are not narrowband signals, specially designed antennas must be used in order to get the normally desired directivity. The problems with high powers and directive antennas are currently being researched. However, applications which can tolerate omni-directional antennas and which operate with small powers (and thus small ranges) can use UWB technology without having very complex or costly systems.

Currently, there are a few companies which are in the process of developing devices which can be manufactured with solid state technology. These devices also use very low transmitted power levels and low gain antennas. One of the companies is Aether Wire and Location, Inc. of Nicasio, California which is developing UWB devices which can perform accurate location. They are very close to coming out with a commercial product. Pulson Communications is developing UWB technology for a time hopping multiple access

communication system [1]. Lawrence Livermore Laboratories has also developed their own UWB technology and is now licensing this technology for various applications [2].

As mentioned above, UWB signals can be used in a time hopping system. Pulson Communications is working on a time hopping system described in [1] which R. A. Scholtz has and analyzed in [3,4]. The basic signal is a pulse train of UWB pulses (called monocycles because they resemble one cycle of a sine wave) where the pulse widths are on the order of a nanosecond and the pulse repetition frequency is on the order of a megahertz. The interval between pulses is then varied by a pseudo-random code. This can be visualized as having each monocycle being "hopped" to different positions within each pulse repetition interval, or frame. The monocycle positions are then slightly shifted again in order to modulate the signal with the information sequence. Thus, this system uses a pulse position modulation (PPM) scheme. This system can support multiple access communications by having each user transmit with its own pseudo-random hopping sequence. As mentioned before, this system can be thought of as the dual of a frequency hopping system. However, the hopping rate is not limited as much as it is in a frequency hopping system, and thus, fast time hopping systems are practical. This allows the system to take advantage of the diversity that fast hopping provides.

UWB signals have some interesting characteristics with are worth mentioning. As with all spread spectrum systems, time hopping systems are able to reject many types of interference. UWB signals are different in that the small pulse widths allow the system to reject (or resolve) multipath components with much smaller path differences than other spread spectrum systems. The small pulse widths also give the system very accurate location information. This allows for a system which can both track and communicate with a mobile receiver. Researchers at the Virginia Tech Center for Transportation Research are examining the application of UWB technology to Intelligent Transportation Systems [5]. One example is an Automated Highway System where communication links

allow processors on the roadside to completely control every vehicle on a highway. It is believed that UWB devices can locate each vehicle with accuracy on the order of centimeters and provide the communication link so that the processors can control the vehicles.

One important consideration is how UWB signals, which have such enormous bandwidths, are going to affect existing narrowband signals. Fortunately, UWB signals have some characteristics which permit them to be overlaid over existing narrowband users. The pseudo-random hopping is very important even in systems without multiple access capabilities because it "spreads" the energy of the signal over the entire bandwidth occupied by a signal pulse. This means that the power spectral density would be much lower than narrowband signals with the same power. Another important point is that UWB signals have very low duty cycles. Finally, current UWB devices are being developed for short range applications and thus have transmitter powers of 100 μW or less. All these facts indicate that UWB systems may cause negligible interference to narrowband users and can be overlaid over them. In fact, contacts at the FCC say that in the near future Part 15 Specifications might be changed to include UWB devices with power limitations. [6] Because of these spectrum issues, it is apparent that UWB devices will never be used for large scale systems. However, for specialized systems, UWB is an emerging technology which is practical and has attractive features.

1.3. Previous Work

As mentioned before, there has not been much research into TH spread spectrum systems. A few researchers like Lam and Sarwate [7] have looked at time hopping multiple access packet communications. A general description of the UWB system is presented in a paper by Withington and Fullerton [1]. The papers by Scholtz [3,4] present an analysis of the UWB system using a Gaussian approximation. Since TH can be thought of as the dual of FH, there are some papers on FH which help to provide insight into the performance of

TH systems. In a paper by Wang and Moeneclaey [8], a fast FH system in a fading channel is analyzed. The paper by Geraniotis [9] presents an accurate analysis of a FH system using characteristic functions.

1.4. Purpose of Thesis

As mentioned before, the UWB time hopping PPM system was studied in papers by Scholtz [3,4]. In these papers, the BER performance of the system is analyzed by using a Gaussian approximation that is very similar to the one used for DS spread spectrum [10]. This analysis yields a very compact result which resembles the result for DS. The purpose of this thesis is to examine the Gaussian approximation presented by Scholtz. Through the use of a novel simulation technique, the Gaussian approximation will be investigated to see how well it applies in certain situations. It will be shown that in certain significant cases, the Gaussian approximation is quite optimistic. An alternative performance evaluation method based on integration of the characteristic function is developed and shown to be more accurate over a wide range of examples. This technique contributes to the understanding of UWB time hopping systems.

1.5. Organization of Thesis

The rest of the thesis will be organized in the following manner. Chapter 2 provides a detailed description of the transmitter and receiver. This will allow for a derivation of the Gaussian approximation in Chapter 3 using a slightly simpler approach than used in [3,4]. Next the simulation method and results will be presented in Chapter 4. These results will show where the Gaussian approximation fails to accurately predict performance. Then, a more accurate analysis using characteristic functions will be presented in Chapter 5. This analysis will also provide some insight into the system and help to explain why the Gaussian approximation fails in certain circumstances. In Chapter 6, reasons why the Gaussian approximation fails will be discussed along with some of the practical implications of the results which were presented throughout the thesis. Finally, a summary

of the results of this thesis and some future research directions will be discussed in Chapter 7.

2. The UWB PPM Time Hopping System

In this chapter, a mathematical model for a time hopping multiple access system which will be used throughout the remainder of this thesis will be introduced. As mentioned before, the UWB PPM time hopping system was described and analyzed using the Gaussian approximation in [3,4]. Thus, most of the discussion of the system and the Gaussian approximation, except when explicitly stated, is based on the model from [3,4].

2.1. Structure of the Transmitter

The signal transmitted by the k^{th} user, $s_k(t)$, in the UWB time hopping multiple access system is given by

$$s_k(t) = \sum_{i=-\infty}^{\infty} p(t - iT_f - c_i^{(k)}T_c - \delta d_{\lfloor i/N_b \rfloor}^{(k)}) \tag{2.1}$$

where $p(t)$ is the pulse shape of the transmitted monocycles. The transmitted pulses are called Gaussian monocycles because they resemble smoothed single cycles of a sine wave. Figure 2.1 shows a plot of the pulse shape, $p(t)$. As one can see from (2.1), the transmitted signal is a pulse train with each pulse being shifted in time by a different amount. The iT_f term separates each monocycle by T_f, the nominal pulse repetition period, or frame period.

The $c_i^{(k)} T_c$ term adds the pseudo-random time hop to each monocycle. The pseudo-random code for the i^{th} monocycle transmitted by the k^{th} user is specified by $c_i^{(k)}$ which is a pseudo-random integer on the interval [0, N_h]. The variable T_c specifies the resolution of the time hops. This time hopping term has several important purposes. First of all, the code provides the interference rejection capability for the system. At the receiver, interference will be rejected because the code will make the interference uncorrelated with the user's signal. When interference rejection is not required (e.g., the system does not require CDMA), the time hopping code is still important. Without it, the user's signal is basically a modulated pulse train with regular intervals between the pulses. The spectrum

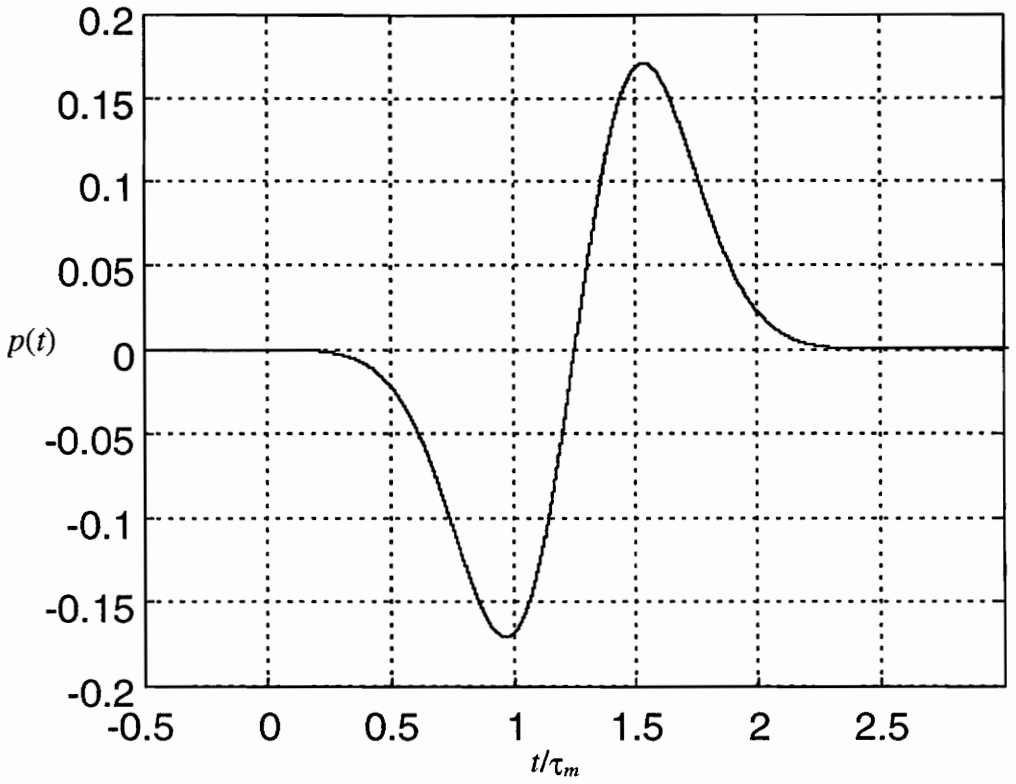

Figure 2.1 - A plot of $p(t)$ vs. t/τ_m

of this signal will be a train of narrowband spikes which will cause significant interference to the narrowband systems which already exist in these bands. The hopping code randomizes the intervals between pulses which causes the energy of the signal to be spread evenly throughout the bandwidth that an individual pulse occupies. Figure 2.2 shows a plot the spectrum of an individual pulse when the pulse width is 1 ns. As can be seen, the bandwidth of the pulse is a few GHz. Thus, the hopping code ensures that the signal will have a large bandwidth and low power spectral density. With the hopping code, the signal is so wideband that it may be considered a baseband signal.

The term $\delta d^{(k)}_{\lfloor i/N_b \rfloor}$ adds the modulation to each monocycle where $d^{(k)}_{\lfloor i/N_b \rfloor}$ is the data bit (0 or 1) which modulates the i^{th} monocycle of the k^{th} user. Thus, no additional shift is

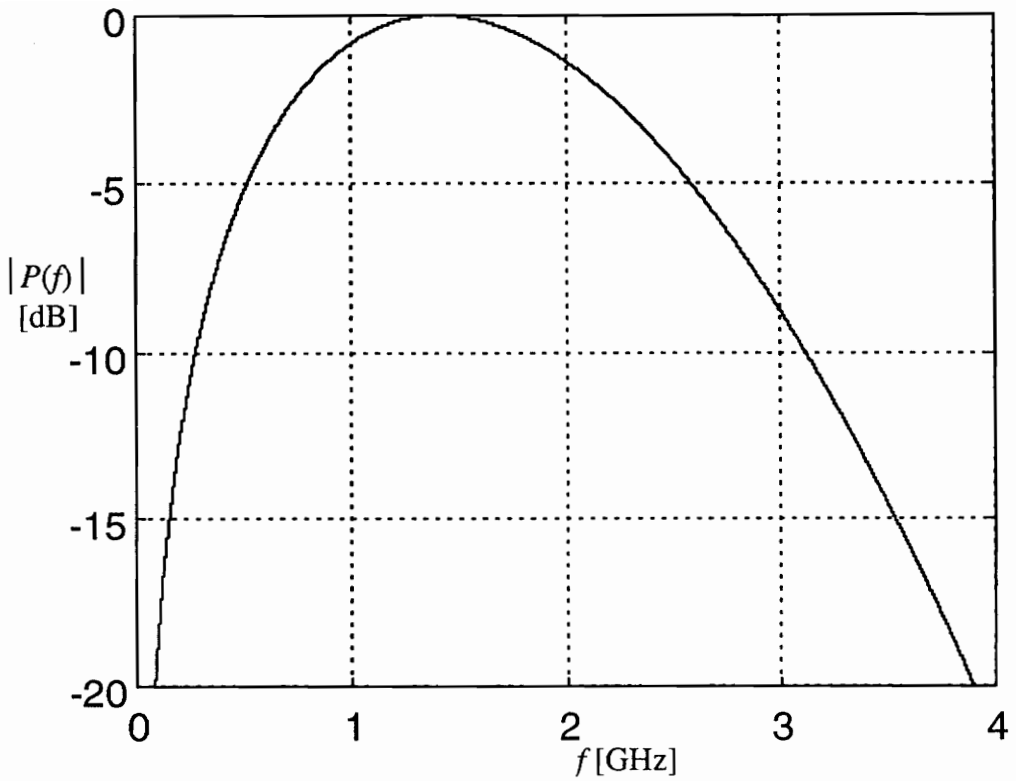

Figure 2.2 - Spectrum of the monocycle, $p(t)$,
when the pulse width is 1 ns

applied when the data bit is a 0, and a shift of δ is applied when the data bit is a 1. As can be seen, this system uses PPM to encode the pulse train with the data stream. The term $\lfloor i/N_b \rfloor$ represents the index of the data bit where $\lfloor \cdot \rfloor$ is the floor function. This means that N_b monocycles will be modulated by the same data bit, and thus, this system is a fast time hopping system.

In order to keep monocycles from hopping into frames other than their own, the parameters of the hopping code must satisfy

$$N_h T_c \leq T_f - T_m - \delta \tag{2.2}$$

where T_m is the width of the monocycle pulse. Also it is easy to show that the bit rate, R_b,

is given by

$$R_b = \frac{1}{N_b T_f}. \tag{2.3}$$

Figure 2.3 shows a block diagram of the transmitter (which is based upon a figure from [3,4]).

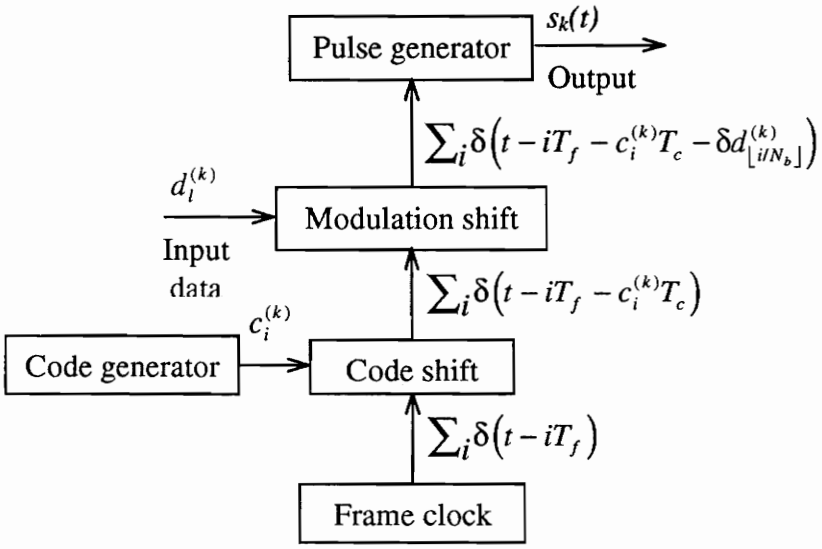

Figure 2.3 - Transmitter Block Diagram

2.2. Channel Model

The channel model used throughout this thesis will be very simple. It will be assumed that the channel causes non-varying attenuation and delay to each user's signal and that the received signal, $r(t)$, is corrupted by additive white Gaussian noise (AWGN), $n(t)$. This simple channel model will help to keep the analyses performed in this thesis simple.

However, this simple AWGN channel model is not that far from reality. There are indications that multipath and Doppler effects will not have as severe an impact on performance as they do in narrowband systems. In fact, the Rayleigh fading which is common in mobile communications only happens with narrowband systems and will not

affect UWB systems [1]. Instead, the Doppler shift will cause the time features of the signal to be expanded or contracted, and the amount of this fluctuation is insignificant even at very large speeds [11]. The only effect which could possibly be significant is the fluctuation of the frame period, but the fluctuations would be small enough to be corrected by a tracking loop. Multipath will not be a big problem since the short pulse width of the system will also cause all but the shortest path differences to become uncorrelated with the original signal. The only potential problem is that the signal power might become so spread out between the multipath components that the performance will be degraded significantly. Solving this problem by using a RAKE receiver might in itself cause more problems. This is because the very small time resolution might make the receiver very complex [3]. This small time resolution also makes the synchronization process more complicated [3].

2.3. Structure of the Receiver

At the receiver, the signal, $r(t)$, due to N_u users and additive white Gaussian noise, $n(t)$, is given by

$$r(t) = \sum_{k=1}^{N_u} \sqrt{P_k}\, r_k(t) + n(t) \tag{2.4}$$

where

$$r_k(t) = \sum_{i=-\infty}^{\infty} w(t - \tau_k - iT_f - c_i^{(k)} T_c - \delta d_{\lfloor i/N_b \rfloor}^{(k)}). \tag{2.5}$$

In (2.4) and (2.5), P_k is the relative received power of the k^{th} user's signal, and τ_k is the relative time delay of the k^{th} user's signal. In (2.5), $w(t)$ is used as the received monocycle's pulse shape. The reason why this is not $p(t)$ is because the monocycles are baseband pulses, and thus, their shape is affected by both the transmitting and receiving antennas as well as the channel itself. All antennas have some frequency dependence which will affect a signal. For narrowband signals, this dependence will not affect the signal; however, for wideband signals, the pulse shape will be altered. For the antennas

normally used in UWB systems, $w(t)$ is approximately the time derivative of $p(t)$. Thus, $r_k(t)$ is approximately the time derivative of a shifted version of $s_k(t)$. When the monocycles are received, their shape is given by

$$w(t+T_m/2)=\left[1-4\pi\left(t/\tau_m\right)^2\right]e^{-2\pi(t/\tau_m)^2} \tag{2.6}$$

where τ_m is a constant which determines the width of the pulse. The term $T_m/2$ is just used to shift the pulse so that the it begins at t=0. Figure 2.4 shows a plot of $w(t)$. As can be seen from this plot, T_m is approximately $2.5\tau_m$. Figure 2.5 shows a plot of the spectrum of $w(t)$.

It is assumed that the receiver has both time and code synchronization with the user's signal which it wishes to demodulate. Thus, the receiver can generate replicas of the two

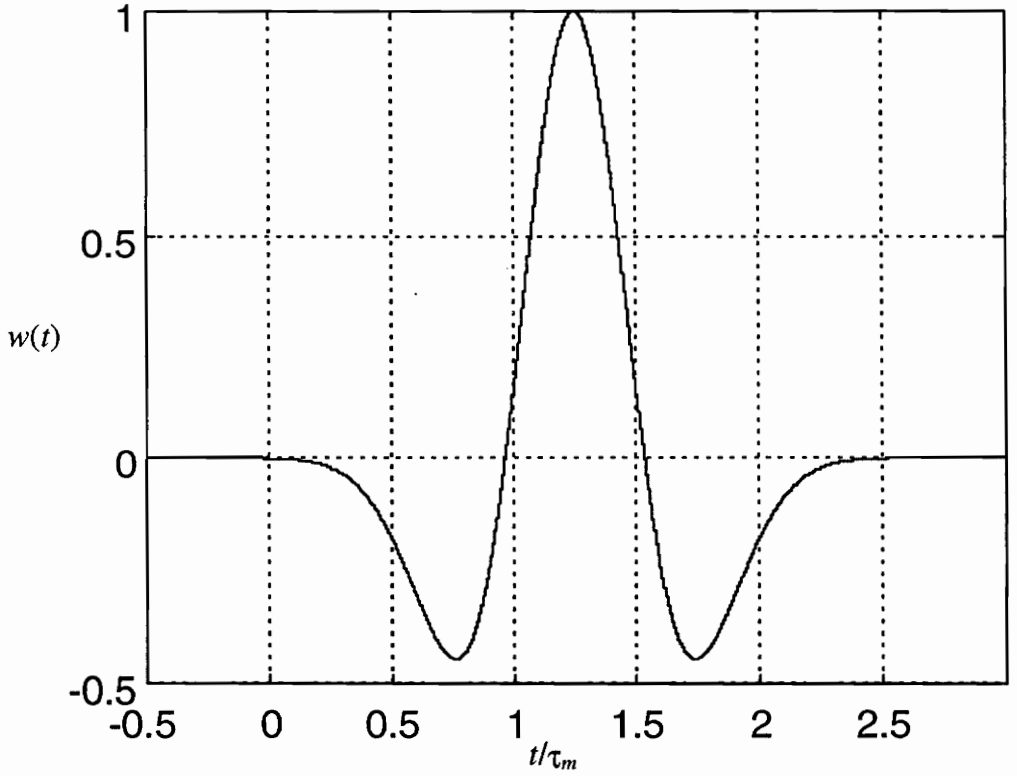

Figure 2.4 - A plot of $w(t)$ vs. t/τ_m

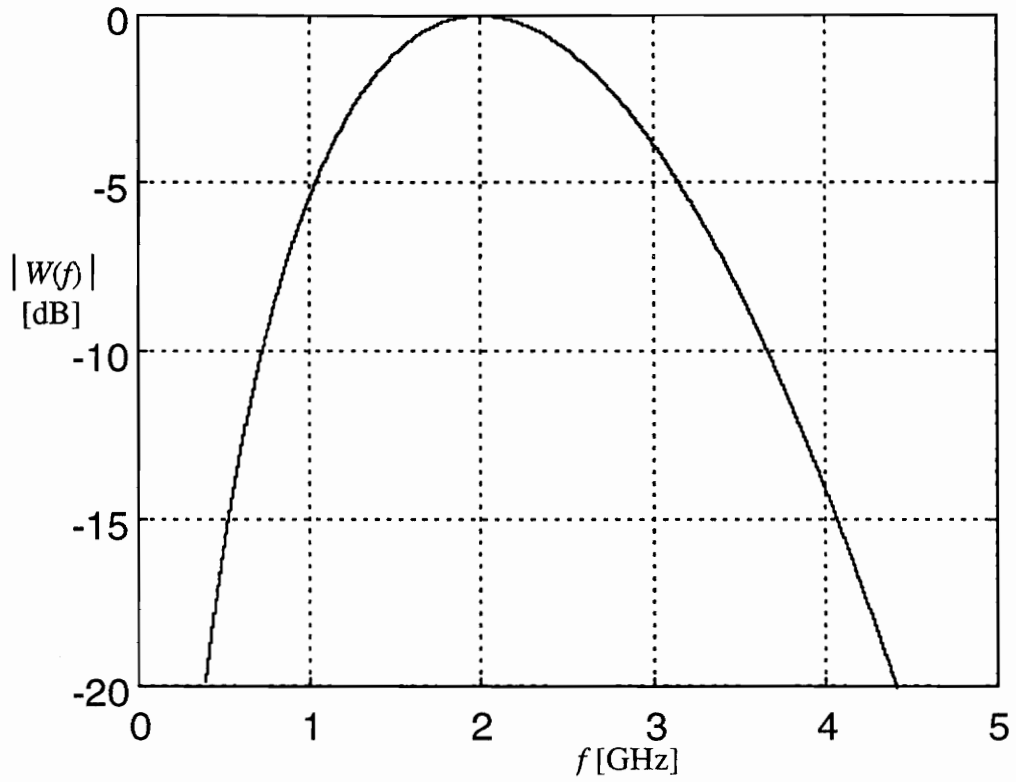

Figure 2.5 - Spectrum of $w(t)$ when the pulse width is 1 ns

possible signals which it can use in a correlation receiver. This is the optimum receiver for that user's signal assuming only AWGN is present. This decision rule is as follows:

$$\text{decide } \hat{d}_l^{(k)} = 0 \text{ if } \int_{\tau_k}^{\tau_k+T_s} r(t) \sum_{i=lN_b}^{(l+1)N_b-1} w(t-\tau_k - iT_f - c_i^{(k)}T_c)dt$$

$$> \int_{\tau_k}^{\tau_k+T_s} r(t) \sum_{i=lN_b}^{(l+1)N_b-1} w(t-\tau_k - iT_f - c_i^{(k)}T_c - \delta)dt\,. \qquad (2.7)$$

By rearranging (2.7), an equivalent but simpler decision rule is given by

$$\text{decide } \hat{d}_l^{(k)} = 0 \text{ if } Z_l^{(k)} = \sum_{i=lN_b}^{(l+1)N_b-1} z_i^{(k)} > 0 \qquad (2.8)$$

where

$$z_i^{(k)} = \int_{\tau_k + iT_f}^{\tau_k + (i+1)T_f} r(t)v(t - \tau_k - iT_f - c_i^{(k)}T_c)dt \tag{2.9}$$

$$v(t) = w(t) - w(t - \delta). \tag{2.10}$$

Hence, only one decision statistic is needed, and this statistic is obtained by summing the correlations of each monocycle with the template signal $v(t)$. Figure 2.6 shows a plot of $v(t)$ when δ/τ_m=0.5. In the next chapter, it will be shown that this value of δ/τ_m is close to the choice which gives the optimal performance. Figure 2.7 shows the spectrum of v(t).

By looking at Figure 2.6, one can see how the template signal will work. When the transmitted data bit is a zero (no shift), then the main lobe of $w(t)$ will line up with the large positive peak of $v(t)$ and the resulting correlation will have a large positive value. When the transmitted data bit is a one (a shift of δ), the main lobe of $w(t)$ will line up with

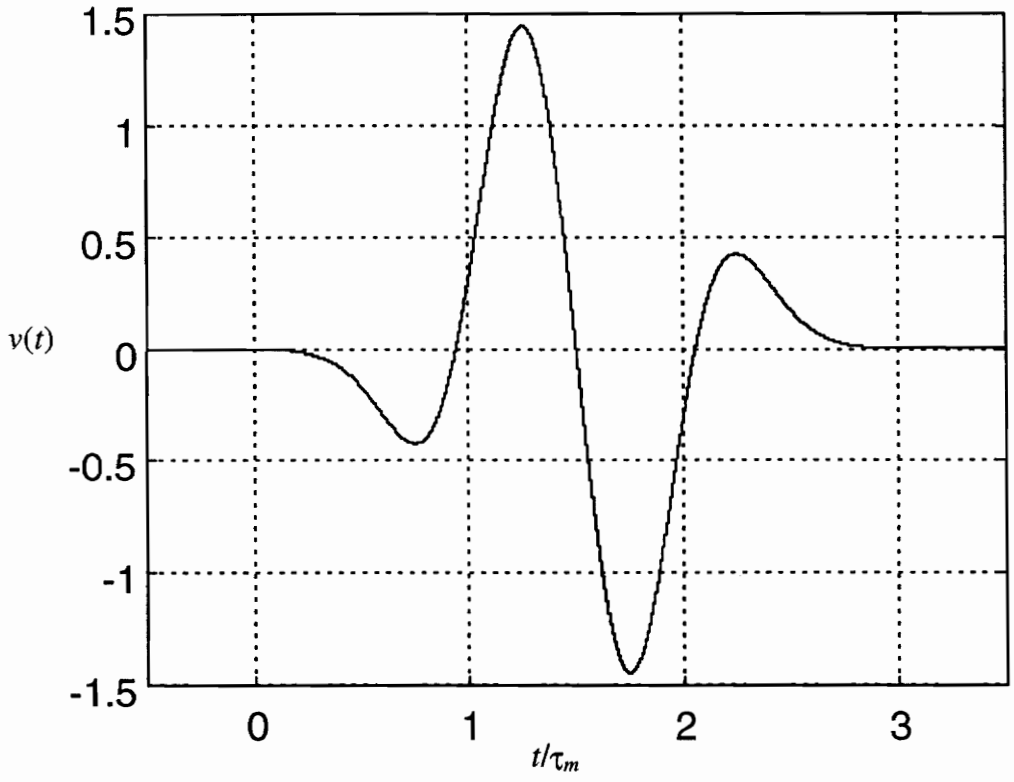

Figure 2.6 - A plot of $v(t)$ vs. t/τ_m with δ/τ_m=0.5

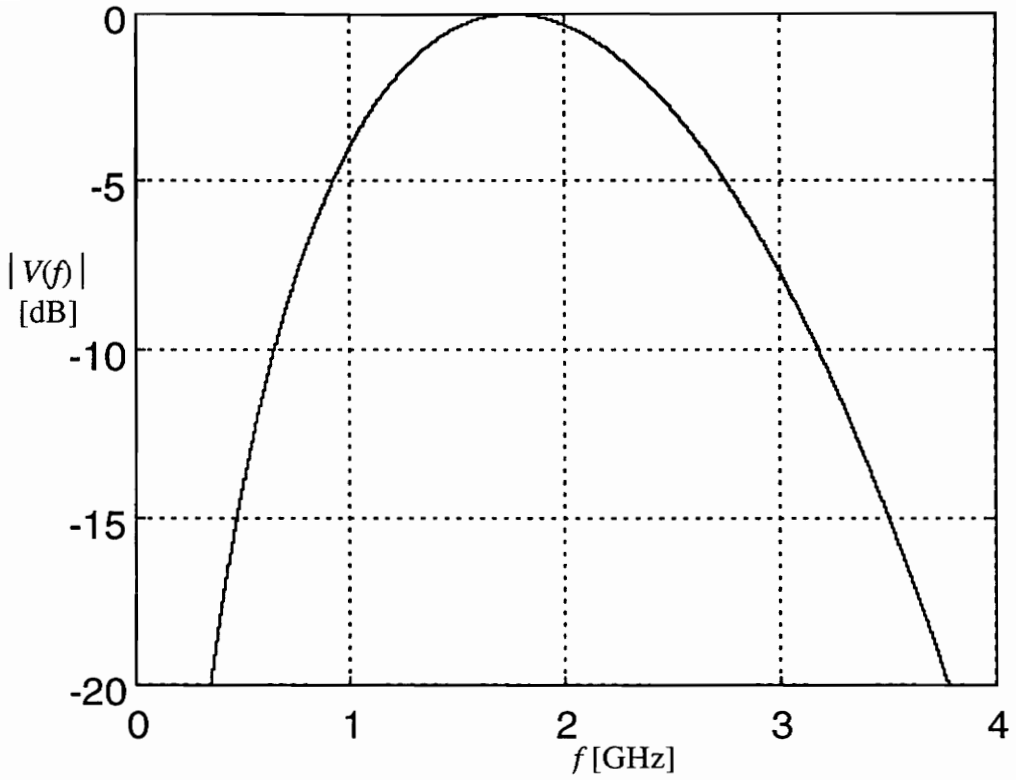

Figure 2.7 - Spectrum of $v(t)$ when the monocycle pulse width is 1 ns and δ/τ_m=0.5

the large negative peak of $v(t)$. The correlation of this signal with v(t) will result in a large negative value.

As with other spread spectrum systems, this receiver is not optimal if the other user's codes are known, but it has good performance and is not very complex. Figure 2.8 shows the block diagram of the receiver taken from [3,4].

2.4. Summary

In this chapter, a simple model for the UWB time hopping system has been presented. In the next chapter, a simple analytical result will be developed for this model using a

Gaussian approximation.

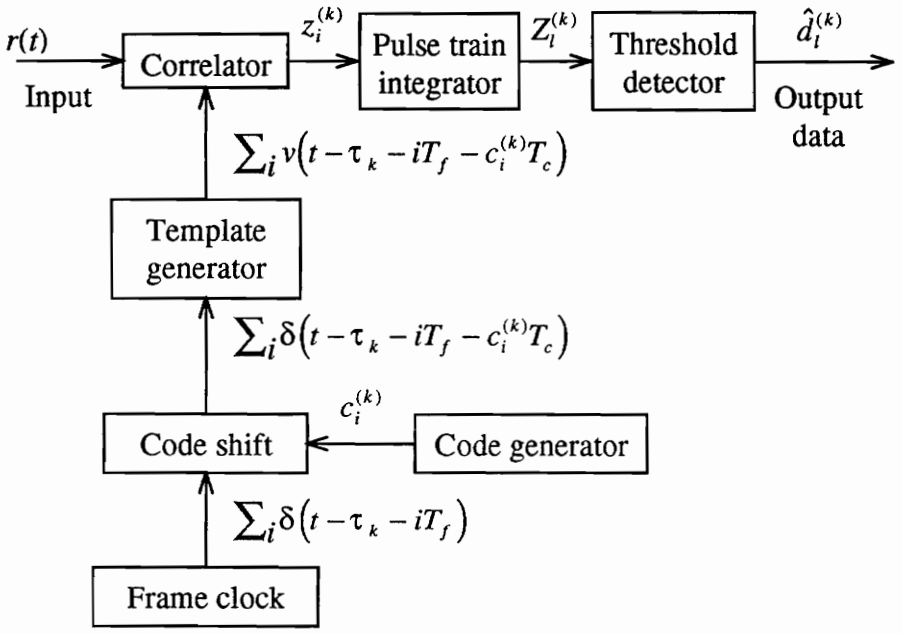

Figure 2.8 - Receiver Block Diagram

3. The Gaussian Approximation

3.1. Using the Gaussian Approximation for the UWB Time Hopping System

As with other spread spectrum systems, a good estimate of the bit error probability for the UWB system can be obtained by assuming the total noise seen at the receiver is Gaussian. This is normally a good approximation when the multiple access interference can be modeled as a sum of a large number of independent random variables. Thus, the noise is approximately Gaussian by the Central Limit Theorem (CLT). In this analysis, it will be assumed that user 1's signal is the desired signal and that the receiver is trying to demodulate $d_0^{(1)}$, the 0^{th} bit. Thus, the decision statistic, $Z_0^{(1)}$, for the receiver will be given by

$$Z_0^{(1)} = m + n_t \tag{3.1}$$

where m is the constant part due to the signal and n_t is random noise. The values of m when $d_0^{(1)}=1$ and when $d_0^{(1)}=0$ are given by

$$m_1 = \sum_{i=0}^{N_b-1} \int_{\tau_1+iT_f}^{\tau_1+(i+1)T_f} \sqrt{P_1} w(t-\tau_1-iT_f-c_i^{(1)}T_c-\delta) v(t-\tau_1-iT_f-c_i^{(1)}T_c)dt \tag{3.2}$$

$$m_0 = \sum_{i=0}^{N_b-1} \int_{\tau_1+iT_f}^{\tau_1+(i+1)T_f} \sqrt{P_1} w(t-\tau_1-iT_f-c_i^{(1)}T_c) v(t-\tau_1-iT_f-c_i^{(1)}T_c)dt\,, \tag{3.3}$$

respectively. By rearranging some terms and performing some variable substitutions, m_1 and m_0 can be simplified to

$$m_0 = -m_1 = \sqrt{P_1} N_b m_p \tag{3.4}$$

where

$$m_p = \int_{-\infty}^{\infty} w(t)v(t)dt = E_w - R_w(\delta) \tag{3.5}$$

and

$$E_w = \tfrac{3}{8}\tau_m \tag{3.6}$$

$$R_w(\tau) = \int_{-\infty}^{\infty} w(t)w(t-\tau)dt = E_w\left[\tfrac{4}{3}\pi^2(\tau/\tau_m)^4 - 4\pi(\tau/\tau_m)^2 + 1\right]e^{-\pi(\tau/\tau_m)^2}\,. \tag{3.7}$$

In (3.5), (3.6), and (3.7) E_w denotes the energy of the monocycle waveform $w(t)$, and $R_w(\tau)$ is its autocorrelation function. The random noise, n_t, is given by

$$n_t = \sum_{i=0}^{N_b-1} \int_{\tau_1+iT_f}^{\tau_1+(i+1)T_f} \left[\sum_{k=2}^{N_u} \sqrt{P_k} r_k(t) + n(t) \right] v(t-\tau_1 - iT_f - c_i^{(1)} T_c) dt . \tag{3.8}$$

Now, in order to use the Gaussian approximation, the mean and variance of n_t (μ_t and σ_t^2) must be determined.

3.2. Determining the Mean and Variance of n_t

In order to find σ_t^2 and μ_t, Sholtz [3,4] uses (3.8) directly and some limiting assumptions on size of $N_h T_c$. However, a simpler method which requires fewer assumptions can be used. First (3.8) is simplified as follows:

$$n_t = n_I + n_o = \sum_{k=2}^{N_u} \sum_{i=0}^{N_b-1} n_i^{(k)} + \sum_{i=0}^{N_b} \int_{-\infty}^{\infty} n\left(t+\tau_1 + iT_f + c_i^{(1)} T_c\right) v(t) dt \tag{3.9}$$

where n_I is the noise due to multiple access interference and n_o is the noise due to the AWGN in the channel. In n_I, the random variable $n_i^{(k)}$ is the interference in the i^{th} monocycle due to the k^{th} user. Because $n(t)$ is zero mean AWGN, the mean and variance of n_o are given by [12]

$$\mu_o = 0 \tag{3.10}$$

$$\sigma_o^2 = \frac{N_b N_o}{2} \int_{-\infty}^{\infty} v^2(t) dt = \frac{N_b N_o}{2} \left[2E_w - 2R_w(\delta) \right] = N_b N_o m_p \tag{3.11}$$

where N_o is the one-sided power spectral density of $n(t)$. Assuming the $n_i^{(k)}$'s are independent (as is done in [3,4]), then the mean and variance of n_I are given by [12]

$$\mu_I = \sum_{k=2}^{N_u} \sum_{i=0}^{N_b-1} \mu_{i,k} \tag{3.12}$$

$$\sigma_I^2 = \sum_{k=2}^{N_u} \sum_{i=0}^{N_b-1} \sigma_{i,k}^2 \tag{3.13}$$

where $\mu_{i,k}$ and $\sigma_{i,k}^2$ are the mean and variance of $n_i^{(k)}$ respectively.

Since $n_i^{(k)}$ is due to "hits" (i.e., when a monocycle overlaps with the correlator's template function), then an appropriate model of $n_i^{(k)}$ is given by

$$n_i^{(k)} = \begin{cases} \sqrt{P_k} R_{wv}(\tau), & \text{given a hit occurs} \\ 0, & \text{given no hit occurs} \end{cases} \tag{3.14}$$

where

$$R_{wv}(\tau) = \int_{-\infty}^{\infty} w(t-\tau)v(t)dt = R_w(\tau) - R_w(\tau - \delta) \tag{3.15}$$

and τ is a random variable which denotes the offset between the interfering monocycle and the template function. In this model, τ is assumed to be uniformly distributed on the interval where $R_{wv}(\tau)$ is non-zero. This interval is denoted as T_R and is approximately $4\tau_m$ when δ is $0.5\tau_m$ (See Figure 3.1). The final piece of information needed is, P_h, the probability of a hit. Assuming each monocycle's position is uniformly distributed over the frame interval, the probability of a hit is given by

$$P_h = \frac{T_R}{T_f}. \tag{3.16}$$

Thus, the mean and variance of $n_i^{(k)}$ are given by [12]

$$\mu_{i,k} = \frac{P_h\sqrt{P_k}}{T_R}\int_{-\infty}^{\infty} R_{wv}(t)dt = 0 \tag{3.17}$$

$$\sigma_{i,k}^2 = \frac{P_h P_k}{T_R}\int_{-\infty}^{\infty} R_{wv}^2(t)dt = \frac{\tau_m E_R P_k}{T_f} \tag{3.18}$$

where

$$E_R = \frac{1}{\tau_m}\int_{-\infty}^{\infty} R_{wv}^2(t)dt = \frac{E_w^2}{72\sqrt{2}}\Big[105 - \Big(105 - 420\pi(\delta/\tau_m)^2 + 210\pi^2(\delta/\tau_m)^4 - 28\pi^3(\delta/\tau_m)^6 + \pi^4(\delta/\tau_m)^8\Big)e^{-\frac{\pi}{2}(\delta/\tau_m)^2}\Big]. \tag{3.19}$$

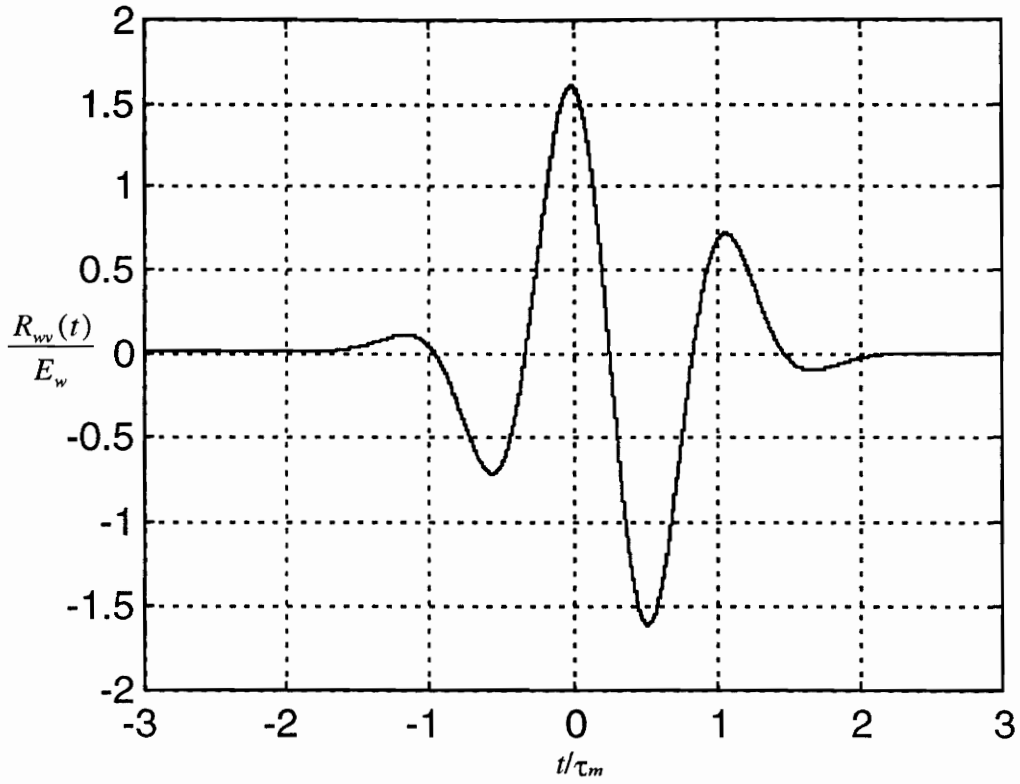

Figure 3.1 - Plot of $R_{wv}(t)/E_w$ vs. t/τ_m for $\delta=0.5\tau_m$

Thus, n_t is a zero mean random variable with variance, σ_t^2, given by

$$\sigma_t^2 = N_b N_o m_p + N_b \left[\sum_{k=2}^{N_u} P_k \right] \frac{\tau_m E_R}{T_f}. \tag{3.20}$$

3.3. Calculating the Probability of Error

If probability of transmitting a "1" or a "0" are both equal to 1/2, then, using the Gaussian approximation, the bit error probability, P_e, can be calculated using

$$P_e = \tfrac{1}{2} P(m + n_t \le 0 \,|\, d_0^{(1)} = 0) + \tfrac{1}{2} P(m + n_t > 0 \,|\, d_0^{(1)} = 1)$$

$$= \frac{1}{2} Q\left(\frac{m_0}{\sigma_t}\right) + \frac{1}{2} Q\left(\frac{-m_1}{\sigma_t}\right) = Q\left(\frac{m_0}{\sigma_t}\right) \tag{3.21}$$

where

$$Q(x) = \frac{1}{\sqrt{2\pi}} \int_x^\infty e^{-t^2/2} dt . \tag{3.22}$$

Putting everything together gives

$$P_e = Q\left(\frac{\sqrt{P_1} N_b m_p}{\sqrt{N_b N_o m_p + \frac{\tau_m E_R N_b}{T_f} \sum_{k=2}^{N_u} P_k}}\right) = Q\left(\frac{1}{\sqrt{\frac{E_w}{m_p}\frac{N_o}{E_b} + \frac{\tau_m}{N_b T_f}\frac{E_R}{m_p^2}\sum_{k=2}^{N_u}\frac{P_k}{P_1}}}\right) \tag{3.23}$$

where E_b is the energy per bit and is given by

$$E_b = P_1 N_b E_w . \tag{3.24}$$

The terms E_w/m_p and E_R / m_p^2 in (3.23) depend only on δ/τ_m, and, thus, a value for δ which minimizes P_e can be found. The term E_w/m_p is the reciprocal of the normalized signal amplitude at the output of the correlator, and the term E_R / m_p^2 is the ratio at the output of the correlator of the normalized power caused by a hit to the normalized signal power. Not only do these factors depend on δ/τ_m, but they will also change if a different pulse shape is used. In Table 3.1 below are some values of E_w/m_p and E_R / m_p^2 for different values of δ/τ_m. The first two rows show the values when E_w/m_p and E_R / m_p^2 are minimized respectively. Thus, the first row values would minimize P_e when the channel noise is dominant, while the values in the second row would minimize P_e when the multiple access interference is dominant. However, as Table 3.1 shows, the values from the first two rows are relatively close together. Since the multiple access interference is normally dominant, the values in the second row are more appropriate. However, in order

to simplify the simulation which will be presented in Chapter 4, a value of δ/τ_m equal to 0.5 will be used throughout this thesis. Table 3.1 shows that this choice does not alter the results significantly.

Table 3.1 - Values of E_w/m_p and E_R / m_p^2 for various values of δ/τ_m

δ/τ_m	E_w/m_p	E_R / m_p^2
0.5408	1/1.618	0.68896
0.5022	1/1.603	0.68265
0.5	1/1.601	0.68267

Substituting these values into (3.23) gives the following:

$$P_e = Q\left(\frac{1}{\sqrt{\frac{N_o}{1.6E_b} + \frac{0.683\tau_m}{N_b T_f}\sum_{k=2}^{N_u}\frac{P_k}{P_1}}}\right). \tag{3.25}$$

Despite the difference in notation, this results from (3.23) and (3.25) are the same as those in [3,4]. However the approach used here uses fewer assumptions and is slightly less complex. Also, parts of the result from [3,4] were done numerically and thus do not explicitly show the dependence on δ and τ_m.

The results of the Gaussian approximation for time hopping look very much like those for DS/SS. If the fact that T_m is approximately $2.5\tau_m$ is used, then (3.25) can be rewritten as

$$P_e = Q\left(\frac{1}{\sqrt{\frac{N_o}{1.6E_b} + \frac{1}{3.7N}\sum_{k=2}^{N_u}\frac{P_k}{P_1}}}\right) \tag{3.26}$$

where N is the processing gain and is given by

$$N = \frac{N_b T_f}{T_m}. \tag{3.27}$$

This result is exactly the same as the result for DS except for the two numerical constants. The 1.6 is a 2 for DS and shows that DS is better when the channel noise is dominant because it uses antipodal signaling. The 3.7 is a 3 for DS and shows that the UWB time hopping system is slightly better at rejecting multiple access interference. This is a crude comparison, however, because the results for DS are for rectangular pulse shaping which is not possible in the UWB system.

Figure 3.2 shows a plot of the Gaussian approximation from (3.26) for various values of N_u with N=100 and all P_k's equal to P_1. This plot is similar to plots used to show the

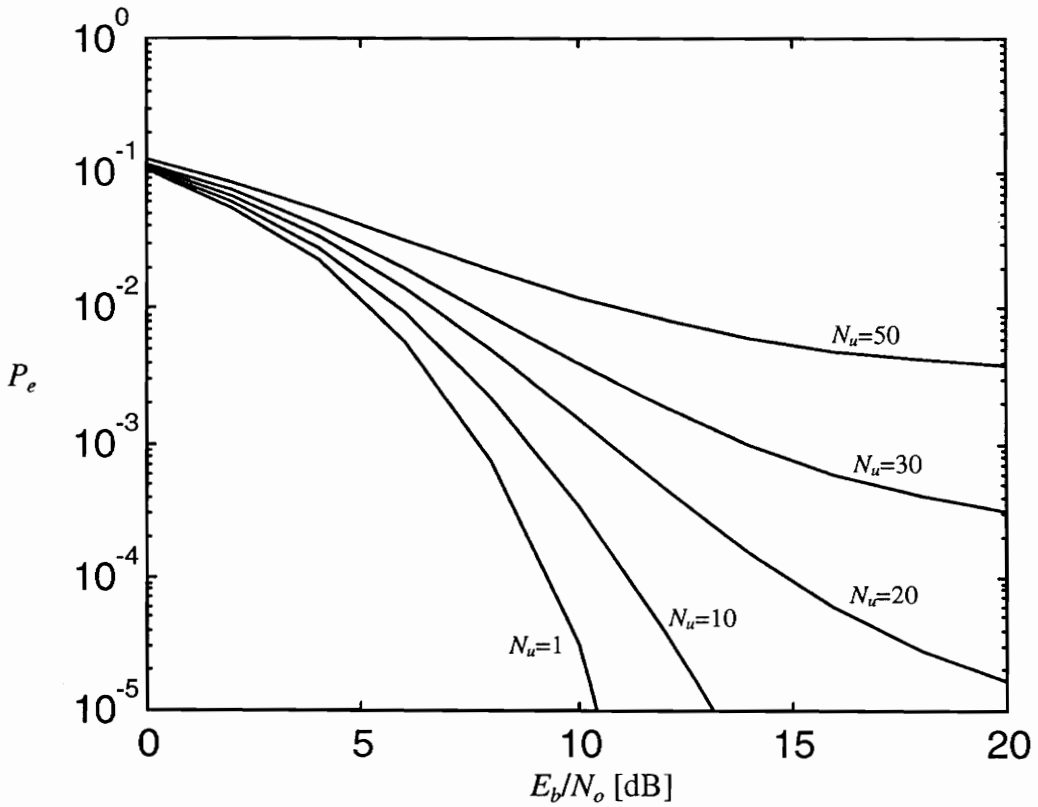

Figure 3.2 - Plot of P_e vs. E_b/N_o for different values of N_u with N=100

performance of DS/SS systems and shows how the performance changes as the number of users increases.

3.4. Summary

In this chapter, a Gaussian approximation has been used to estimate the performance of the UWB time hopping system. This has led to an analytical result which is rather simple. In the next chapter, a simulation of the UWB time hopping system will be used to see how well the Gaussian approximation predicts performance in various situations.

4. Simulation of the UWB PPM Time Hopping System

4.1. Purpose of the Simulation

When one has analytical results for the performance of a communication system, then it is fair to ask why simulation results are needed. A typical answer would be that they are needed to verify the analytical results. For the case of the UWB/TH system, this answer is justified because the analytical results are based upon assumptions and approximations. This is not to say that some of the assumptions are possibly unwarranted, but sometimes assumptions will only apply in certain idealized circumstances. Thus, by showing under what circumstances the analysis is valid, simulation can provide valuable insight into the system performance.

For the UWB/TH system specifically, there are indications that the Gaussian approximation might not be valid under some circumstances. The CLT applies for all but pathological distributions (e.g. distributions with infinite moments); however, it will not apply if the random variables being summed are dependent. Thus, if some of the assumptions on independence are not valid, then the Gaussian approximation could provide incorrect results. This problem is seen in the Gaussian approximation of the performance of DS/SS. Some papers [13,14] have shown that the Gaussian approximation is optimistic in certain situations because the multiple access interference is dependent on the desired user's spreading sequence. Another important consideration is that the CLT only guarantees convergence and does not specify how the convergence rates vary between distributions. Because the statistics of the multiple access interference for UWB/TH system are complicated, there is a chance that characteristics of the true distribution will affect the convergence in certain situations.

4.2. Simulation Method

The usual approach to simulation of communication systems is to find a suitable sampling frequency and represent the signals in digital form. If the RF signals are being simulated,

then the complex envelope representation can be used to transform these signals into baseband equivalents. The system is simulated by sequentially processing the digital signal using mathematical models for each component of the system. A Monte Carlo BER simulation would then, using the correct decision rule, decide upon the received sequence of bits and calculate the number of errors that occurred in the decision process. This approach leads to very long simulations for spread spectrum systems because of their large bandwidth. However, with the UWB/TH system, the low duty cycle means that the information content of the signal is contained is small periods of time. Thus, much of the generated digital signal is not used to determine performance. The UWB/TH system also does not fit into the normal simulation strategy because it uses wideband signals. Thus, the complex envelope representation is not appropriate because it can only be used for narrowband signals.

Because of the above reasons, a somewhat unorthodox simulation approach was used. First, all the random variables which determine the received signal due to each user, i.e. $c_i^{(k)}$, $d_l^{(k)}$, and τ_k, are generated. Next, for each frame of each user it is determined whether there is a hit from another user and if there is, then the appropriate interference is added to the decision statistic. Finally, the appropriate amount of AWGN is added, and the decision process continues as it would for the conventional method. Thus, the transmitted signal is never generated, and the receiver decision statistic is generated directly using knowledge of the structure of the received signal. To be precise, the decision statistic is calculated using (2.8) with (2.9) simplified to give

$$z_i^{(k)} = \sum_{u=1}^{N_u} \sqrt{P_u} \int_0^{T_m+\delta} w\left(t - \tau_u + \tau_k + (i-m)T_f + \left(c_i^{(k)} - c_m^{(u)}\right)T_c - \delta d^{(u)}_{\lfloor m/N_b \rfloor}\right) v(t)\,dt$$

$$+ \int_0^{T_m+\delta} n\left(t + \tau_k + iT_f + c_i^{(k)} T_c\right) v(t)\,dt \qquad (4.1)$$

where

$$m = \left\lfloor \left(iT_f - \tau_u + \tau_k + c_i^{(k)} T_c \right) / T_f \right\rfloor . \tag{4.2}$$

When it needs to be determined whether or not a hit occurs, the simulation just needs to check if the argument of $w(t)$ in (4.1) is in the interval $[0,T_m]$. Also, since the signals are digitized, the integrals in (4.1) are simply computed using sums. Figure 4.1 shows a general block diagram of the simulation approach used here.

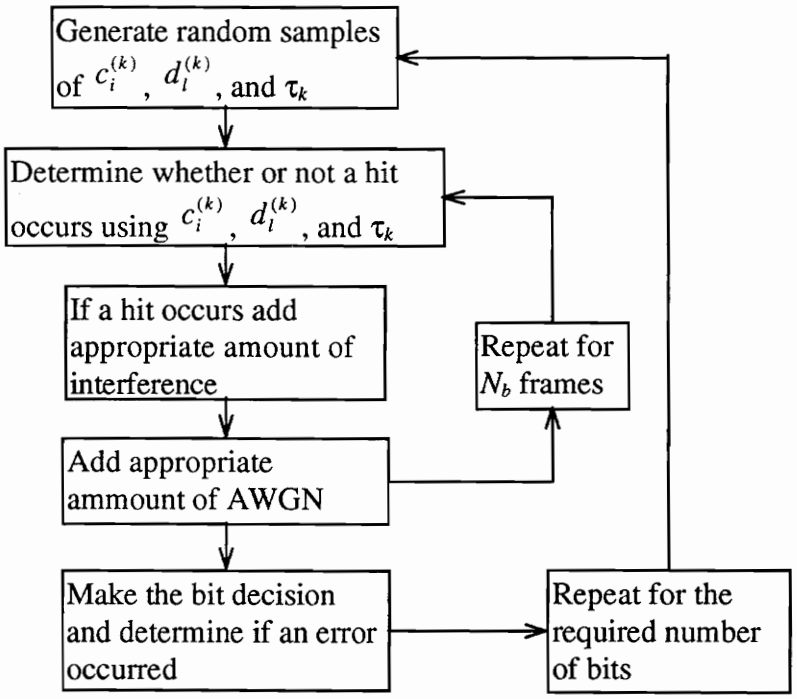

Figure 4.1 - Block diagram for the simulation approach

This method reduces the simulation time significantly, and it also makes the run time relatively independent of T_f. The drawback of this approach is that it is very specialized to the particular system configuration and channel model. Slightly more sophisticated channel models would be nearly impossible to incorporate into this method. Also, because this method is not modular, any changes the system or channel models require wholesale changes to the simulation code.

4.3. Simulation Implementation

The first thing that must be specified in this simulation is the structure of the signals. Even though the transmitter and channel will not be explicitly implemented, the signal structure needs to be known in order to construct the received signal in the receiver. As with all communication system simulations, only changes in the relative time scaling will affect the results. Thus, one particular absolute scaling can be simulated, and the results can be applied to other systems with similar relative scaling. In these simulations, the time was scaled so that the sampling frequency was equal to 1 sample/s. In order, to get a relatively fine time resolution, the width of the received monocycle pulse, T_m, was set equal to 25 samples. This choice will not significantly increase the simulation time because the simulation time will be approximately independent of T_f. Because T_m is approximately $2.5\tau_m$, τ_m was set equal to 10 samples. Because the smallest time shift possible is 1 sample, δ must be an integer multiple number of samples. A value of δ/τ_m equal to 0.5 makes this constraint easy to satisfy, and thus, δ was set equal to 5 samples. This is why the value of δ/τ_m was set equal to 0.5 in Chapter 3.

As mentioned above, there are no distinct modules which implement the transmitter and channel. However, the parameters which describe them ($d_l^{(k)}, c_i^{(k)}$, τ_k, and $n(t)$) must be specified. Since $d_l^{(k)}$ is the bit stream for each user, it is generated using a binary random variable with the probability of a one or zero being equal. As mentioned in Chapter 2, $c_i^{(k)}$ is a random integer uniform on [0, N_h], and in order to get the largest number of hopping positions, T_c is set equal to 1 sample. Then using (2.2), the maximum possible value of N_h is chosen. Since offsets between users can only determined to the nearest bit, the τ_k's will be generated using a random integer uniform on [0, N_bT_f-1] where N_bT_f is in terms of the number of samples. The channel noise $n(t)$ is AWGN so that its samples are generated using independent, zero mean Gaussian random variables. The variance of

these random variables is determined from the value of E_b/N_o being simulated. For discrete samples of an AWGN process, the variance of the noise is given by [15]

$$\sigma^2 = \frac{N_o f_s}{2} \tag{4.3}$$

where f_s is the sampling frequency and N_o is the one-sided power spectral density. Using (3.24) and the fact that f_s is 1 sample/s, (4.3) can be rewritten as

$$\sigma^2 = \frac{3\tau_m N_b}{16 E_b/N_o}. \tag{4.4}$$

To prevent the simulation from only examining one fixed case, each user's bit stream is divided into small blocks with new τ_k's being generated for each block. The number of bits per block per user for which decision statistics are generated will be 2 less than the number of bits in a block. The two unused bits will be the first and last bits in the block, and they are only used to simulate interference for other users. Many of the simulations were run for the case of equal powers for all users. The simulation times for these cases were reduced significantly by determining the bit errors for all the users rather than one particular user. Also, all the simulations were run for a fixed number of errors rather than a fixed number of bits. Again, this decreases the simulation time by only simulating the number of bits which are needed to get a desired accuracy. The error limit for all simulations was set to 100 errors. This value leads to BER results which are at most off by a factor of 1.3 (with a 99% confidence interval) [15].

4.4. Simulation Results

In the following simulation results, systems with $N_b T_f$ equal to 480 and 960 samples were used. These values were chosen because they have a large number of integer factors. Thus, many different systems with the same processing gain but different values of N_b can be simulated. The value of processing gain for these systems is less than the values that are being proposed for practical systems. However the results seen here can be easily

extended to systems with different processing gains.

The first set of results is shown in Figure 4.2. This is a plot of P_e vs. E_b/N_o for different values of N_u with N_b=6 and T_f=80. This type of plot is commonly seen in discussions on other type of spread spectrum because it shows how the performance is affected by the number of users. The simulation results show that the Gaussian approximation estimates the performance well but seems to be consistently optimistic.

Figures 4.3 and 4.4 show plots of P_e vs. E_b/N_o for different values of N_b with N_u=6 and N_bT_f=480. Figures 4.5 and 4.6 are similar plots with N_u=11 and N_bT_f=960. These plots show some interesting results. Whereas the Gaussian approximation predicts the same

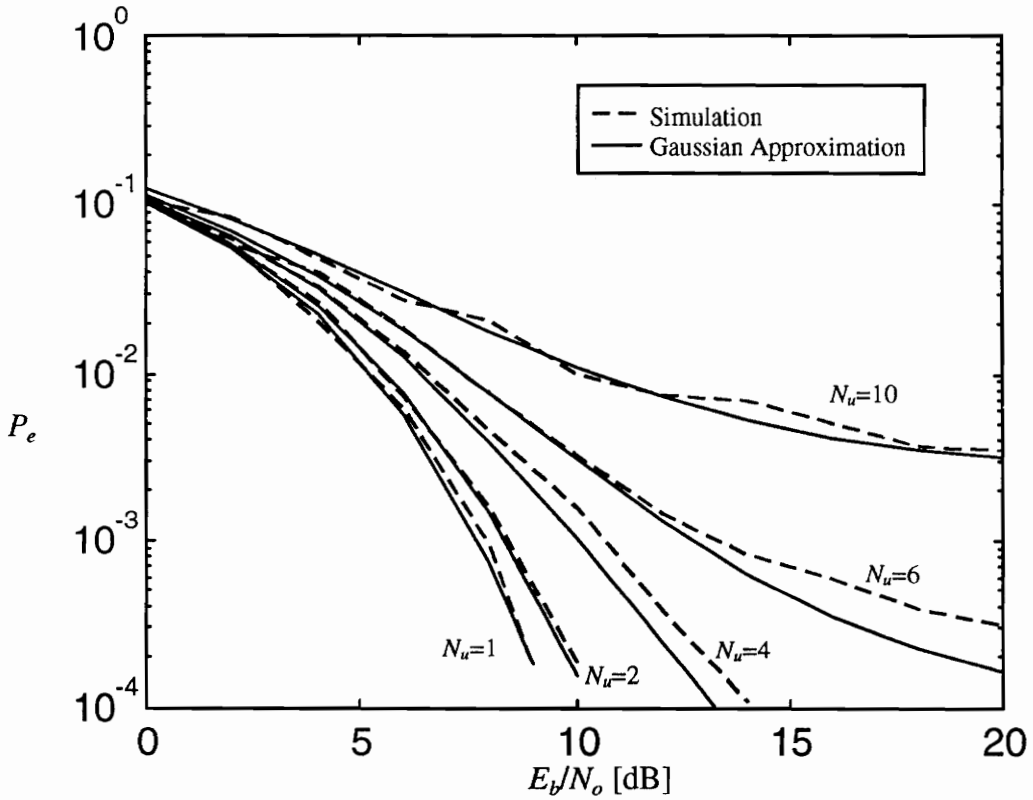

Figure 4.2 - Plot of P_e vs. E_b/N_o for different values of N_u with N_b=6 and T_f=80

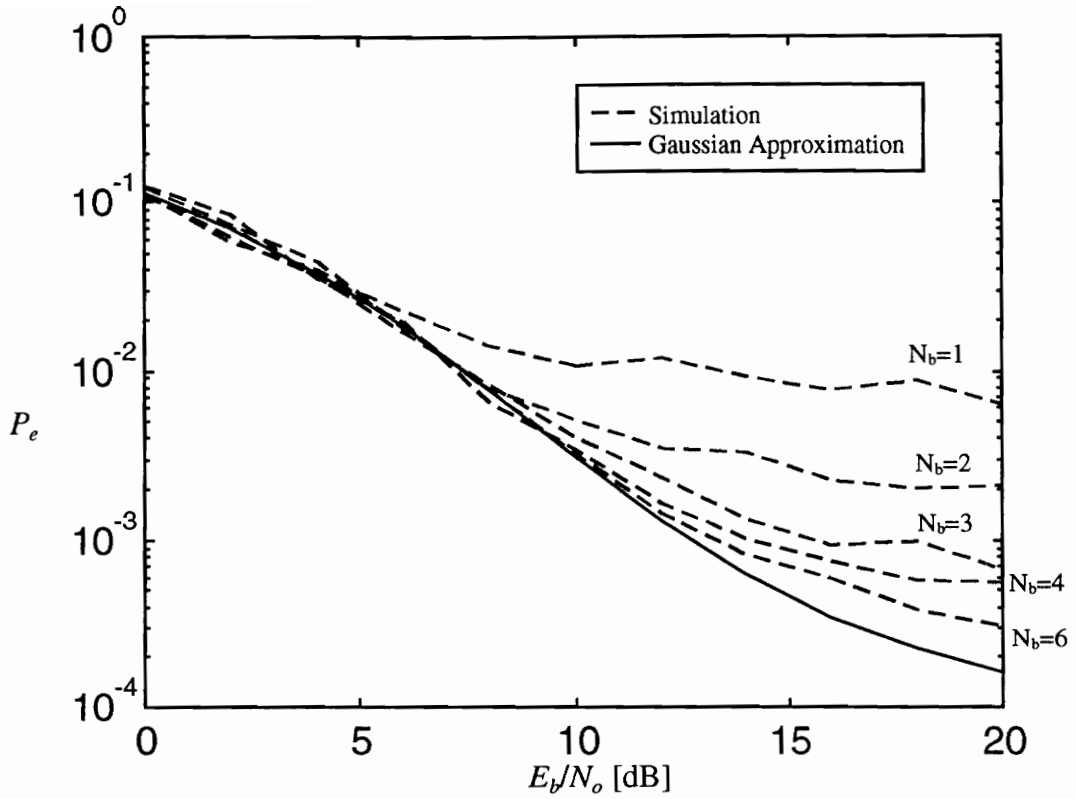

Figure 4.3 - Plot of P_e vs. E_b/N_o for different values of N_b with N_u=6 and N_bT_f=480

performance as long as the product of N_b and T_f is constant, the simulation results show that the performance is dependent on N_b, the number of monocycles per bit. Figures 4.3 and 4.5 show that the P_e for N_b=1 is much worse than what is predicted by the Gaussian approximation. As N_b increases, the performance improves and approaches the performance predicted by the Gaussian approximation. As Figures 4.4 and 4.6 show, the performance remains close to the Gaussian approximation until a certain point. As N_b increases beyond this, the performance again degrades. Actually, the degradation of performance for high N_b is not too surprising. This is because the corresponding frame size at which the performance starts to degrade for Figures 4.4 and 4.6 is about 48 samples. The corresponding values of T_R and T_m for this system are 40 and 25

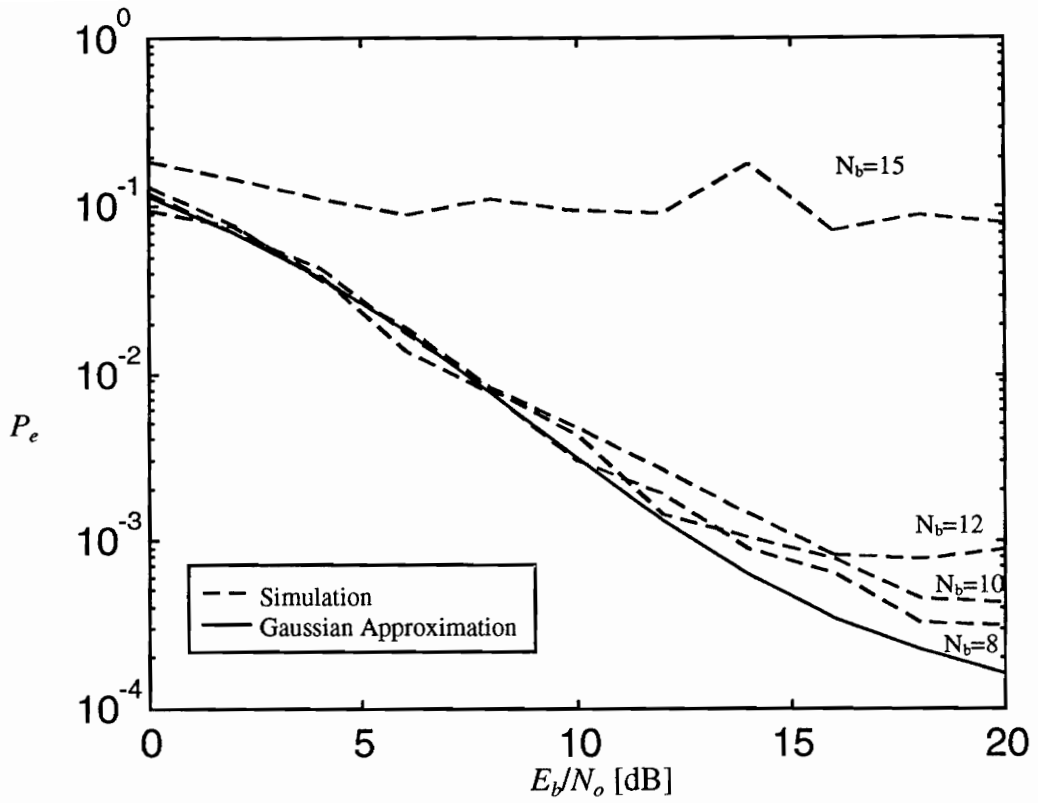

Figure 4.4 - Plot of P_e vs. E_b/N_o for different values of N_b with N_u=6 and N_bT_f=480

respectively. Thus, the degradation in performance is due to the fact that the frame size is barely larger than the monocycle width. Thus, each user is always hit by each other user, and no real multiple access interference rejection is achieved. Small frame sizes have the effect of making it more likely that each monocycle will hit more than one monocycle. Thus, by looking back at the derivation of the Gaussian approximation, one can see that small frame sizes will cause the independence assumption for the $n_i^{(k)}$'s to be violated.

What is more curious and practically important is that the performance degrades when N_b becomes small. One might not expect this since a small N_b (and thus a large T_f) leads to both a smaller probability that an individual monocycle will be hit and a smaller number of

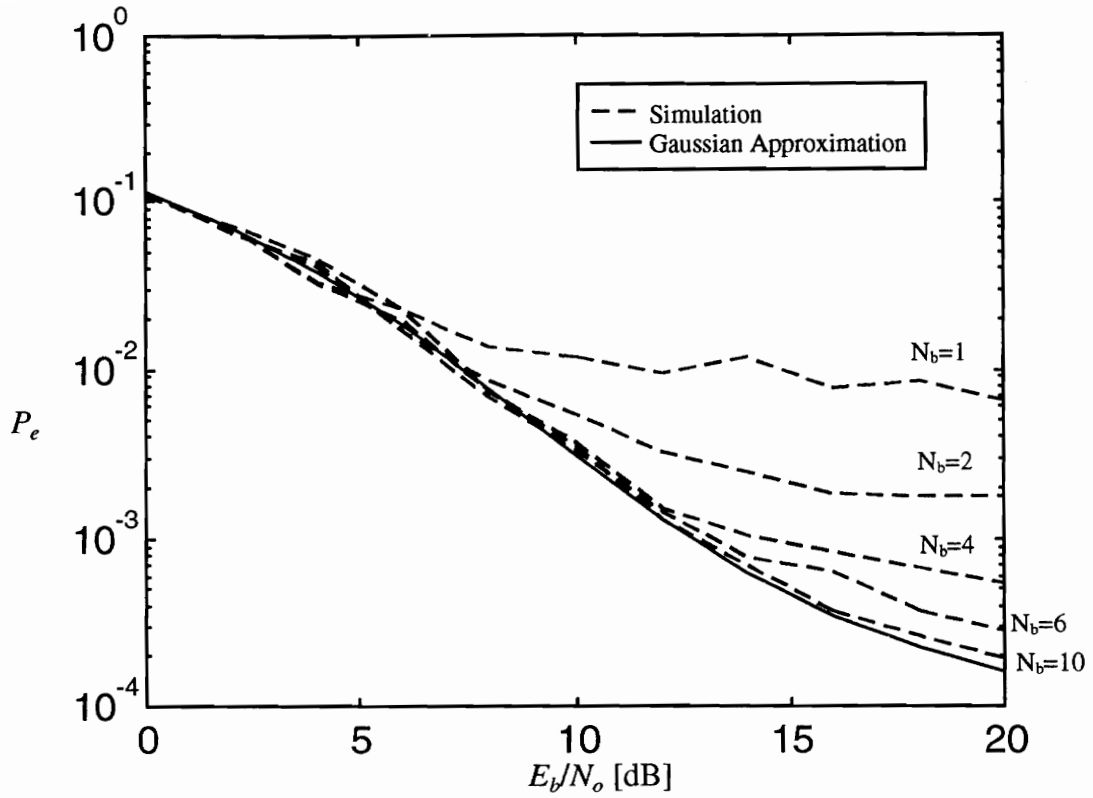

Figure 4.5 - Plot of P_e vs. E_b/N_o for different values of N_b with N_u=11 and N_bT_f=960

monocycles per bit which could be hit. Since the total number of $n_i^{(k)}$'s is N_bN_u, one would expect that the convergence properties would improve as N_b is increased. However, the results from Figures 4.3 and 4.5 are for N_u=6 and N_u=11, and one would expect that the results (even for N_b=1) would be somewhat closer to the Gaussian approximation. Other systems like DS/SS have performance which is not correctly predicted by the Gaussian approximation because the interference is only conditionally independent. However, intuitively it seems that this should not be the case for TH systems. In fact, as presumed above, it seems that the independence assumptions are more valid when N_b is decreased (and T_f is increased).

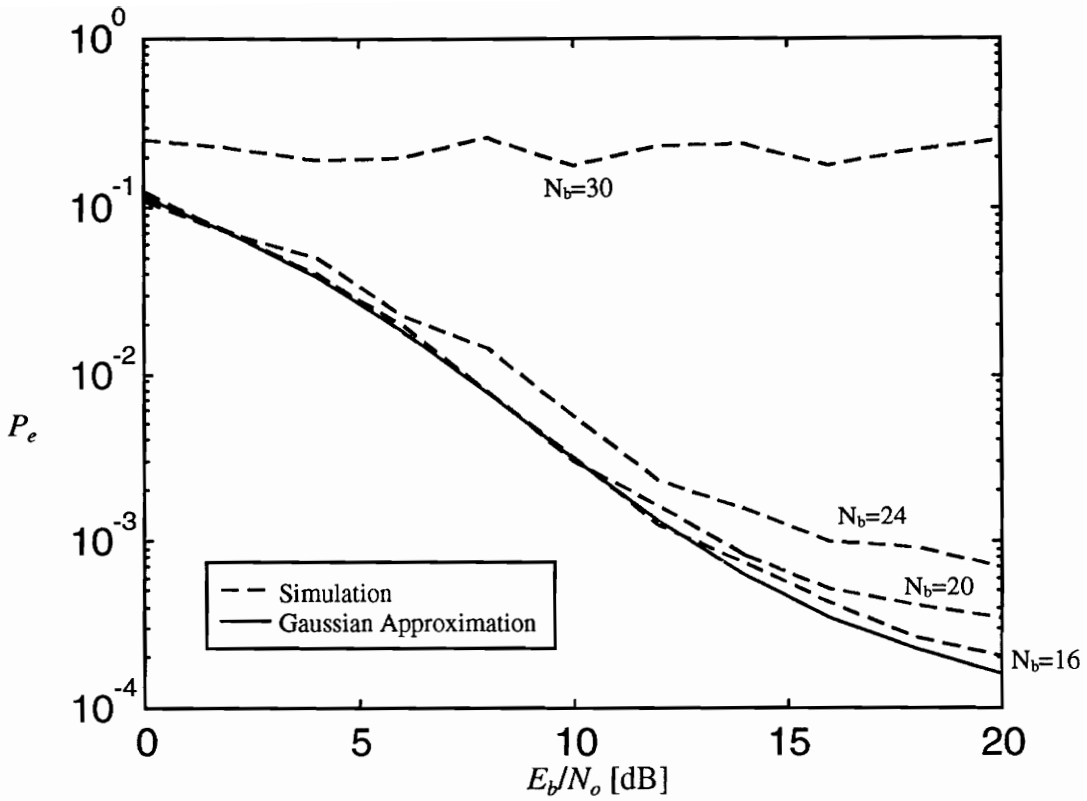

Figure 4.6 - Plot of P_e vs. E_b/N_o for different values of N_b with N_u=11 and N_bT_f=960

Figures 4.3, 4.4, 4.5, and 4.6 also show how the relationship between processing gain and the number of users effects performance. These two systems had the values of N_bT_f and N_u set so that the Gaussian approximation would predict the same performance for both. Thus, each user's signal should experience the same relative amount of interference in both systems. For small values of N_b, the simulation results of the two systems for the same values of N_b are very similar. However, as N_b increases, the performance for the system with N_bT_f=480 degrades sooner because the frame sizes for this system are smaller than those of the other system for equal N_b's. For large values of N_b, the performance of the two systems is similar for the same values of T_f. Thus, as long as the frame size is not too small (which would be of no practical interest anyway), the performance of systems

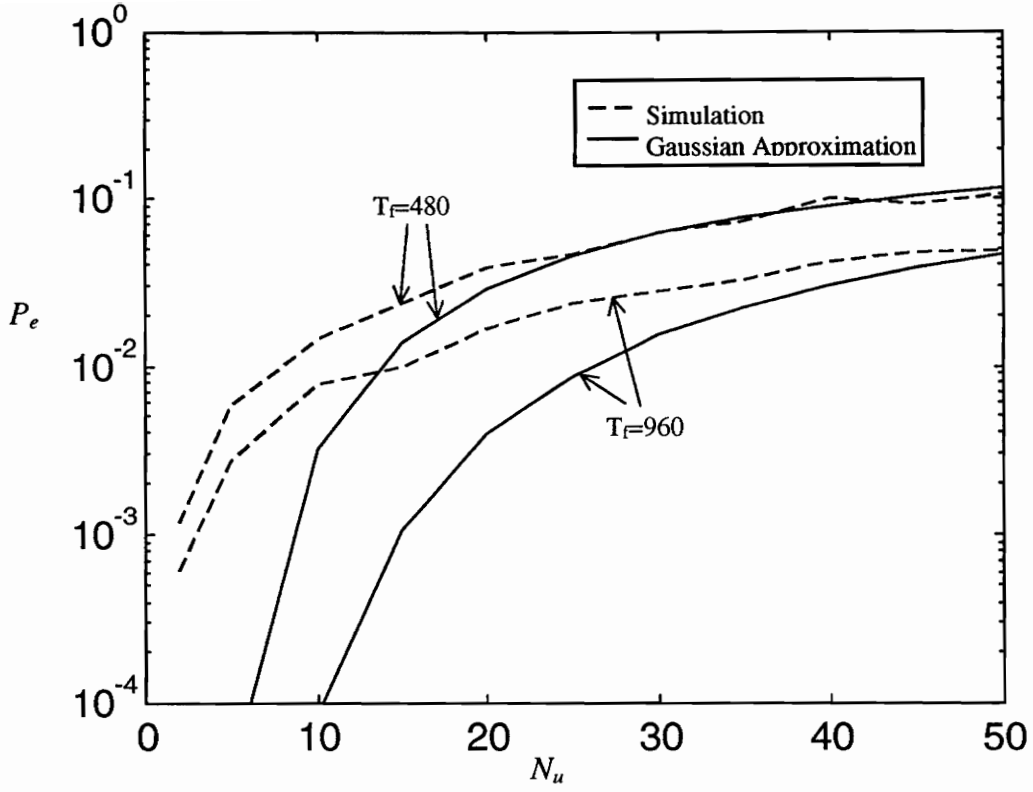

Figure 4.7 - Plot of P_e vs. N_u for different values of T_f with N_b=1 and E_b/N_o=20 dB

with the same relative amount of interference will be similar.

Figure 4.7 is interesting because it shows how the number of users affects the convergence of the Gaussian approximation. This figure is a plot of P_e vs. N_u for different values of T_f with N_b=1 and E_b/N_o=20 dB. The plot shows that, as expected, the results do converge to the Gaussian approximation as the number of users increases. However, the rate of convergence depends upon the value of T_f. The plot shows that increasing the value of T_f by a factor of two doubles the number of users needed for the results to converge to the Gaussian approximation. These results suggest that there is something which causes the convergence properties of the Gaussian approximation to change as T_f is changed.

Figure 4.8 is a plot which looks at how the relative powers of the users affects performance. It is a plot of P_e vs. P_k/P_1 for different values of N_b with N_u=6, N_bT_f=480, and E_b/N_o=20 dB. Here P_1 represents the relative power of the desired user while the other N_u-1 users have equal relative powers denoted by P_k. As before the Gaussian approximation predicts performance which is independent of N_b, and as before the simulation results show that this is not the case. It seems, as before, that the simulation results become closer to the Gaussian approximation when N_b increases. It is interesting that lower values of N_b have better performance than larger values when the multiple access interference is relatively large. For moderate and small levels of multiple access interference, larger values of N_b have better performance which is what was shown in the

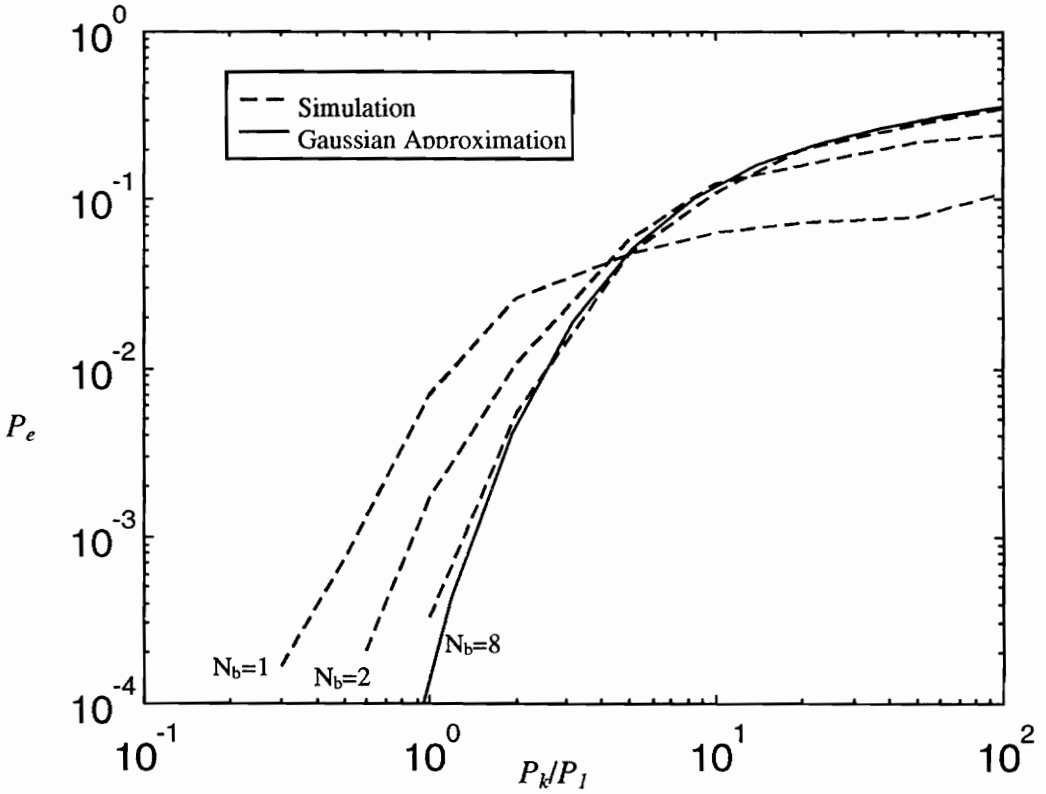

Figure 4.8 - Plot of P_e vs. P_k/P_1 for different values of N_b with N_u=6, N_bT_f=480, and E_b/N_o=20 dB

previous figures. An intuitive explanation for this is that when the multiple access interference becomes very large, it is better to avoid hits rather than trying to average out their effects. This corresponds to choosing a small value of N_b. This same type of relationship was also shown to occur in fast FH systems in a paper by Wang and Moeneclaey [8]. There it was shown that, for a fixed bandwidth, it is better to have one hop per symbol (and, thus, the largest number of hopping frequencies) when the multiple access interference is strong. When the multiple access interference is small, it is better to have a larger number of hops per symbol in order to obtain more diversity.

4.5. Summary of Results

In this chapter it has been shown through simulation that the standard Gaussian approximation for the performance of a TH/SS system is optimistic under certain conditions. In the next chapter, an improved performance evaluation technique based on characteristic functions will be demonstrated.

5. A Numerical Analysis of the UWB PPM Time Hopping System

5.1. Purpose of the Analysis

As was shown in Chapter 4, the Gaussian approximation of the performance of the UWB TH system does not predict some important details that were seen in the simulation results. The obvious next question is whether or not a more accurate analysis method can be developed. Not only would such a method predict the performance more accurately, but it could possibly provide insight into some of the unexpected simulation results.

The results from Chapter 4 seemed to indicate that the Gaussian approximation failed in certain circumstances not because of dependence between hits but because of some other mechanism due to the statistics of the interference. In other words, there were situations where, even though there were a moderate number of random variables contributing to the interference, the high-order moments of the interference were not sufficiently small. It was also shown in Chapter 4 that the convergence rate depends on the value of T_f, and thus, T_f might be affecting the high-order moments in some manner. Another point, which is shown in Figure 5.1, is that the individual components of the interference have large high-order moments. Figure 5.1 is a plot of the cumulative distribution function (cdf) of $R_{ww}(\tau)/E_w$ which is denoted by R in the plot for simplicity. This plot was generated numerically by using 1,000,000 samples of R because there is no analytic expression for the cdf or probability density function (pdf). This random variable represents the interference caused by one hit. As can be seen from Figure 5.1, R has a very non-linear distribution and thus large high-order moments. All these observations lead to the conclusion that an analysis which uses the entire distribution of the interference, rather than only its first and second moments, might provide an accurate prediction of system performance.

5.2. Analysis Method

As proposed above, the improved analysis will model the entire distribution of the multiple

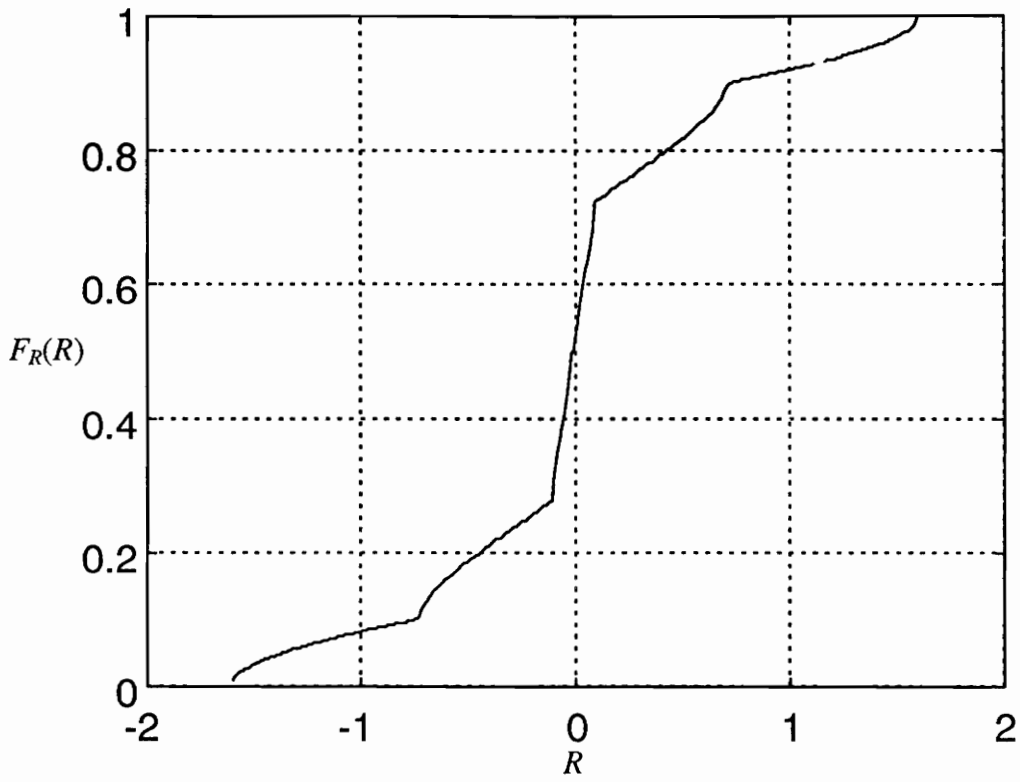

Figure 5.1 - Plot of the cumulative distribution function of $R_{wv}(\tau)/E_w$

access interference. This analysis will be a numerical analysis because there is no closed-form expression for the distribution of R, which is a fundamental component of the total distribution. In fact, the data that was used to generate Figure 5.1 will used to model the distribution of the interference. The distribution of the interference also includes the sum of a number of independent random variables. Thus, in order to compute the total distribution, a number of numerical convolutions would have to be performed. Because convolutions are very numerically intensive, this analysis will use characteristic functions to model the interference. This is the same method that was used in a paper by Geraniotis [9] to analyze the performance of FH/SS. By using this method, the total characteristic function of the interference can be determined analytically because all the convolutions become simple multiplications. Then, the total distribution is obtained by performing one

numerical integration. By using this method, the time required to calculate the performance is kept within a reasonable range.

5.3. Modeling the Characteristic Function of R

As can be seen from Figure 5.1, the distribution of R almost looks like a piecewise linear function. This would suggest that a linear spline approximation would be an appropriate model for the distribution. As will be seen shortly, this model also has a characteristic function which is relatively simple. In order to keep the model simple only 9 unequally spaced linear segments were used. The linear spline, S, can be expressed as [16]

$$S(R) = F_i + \left[\frac{F_{i+1} - F_i}{R_{i+1} - R_i}\right](R - R_i) \quad \text{for } R \in [R_i, R_{i+1}],\ i = 0,\ldots,8 \tag{5.1}$$

where the R_i's are the points where the spline interpolates $F_R(R)$, and the F_i's are the values of $F_R(R_i)$. Table 5.1 shows the values of R_i that were chosen, and Figure 5.2 shows the spline which results from these choices. These values lead to an absolute error which is less than 0.017 for all values of R.

Table 5.1 - Values of R_i used for the linear spline approximation to $F_R(R)$

i	0	1	2	3	4	5	6	7	8
R_i	-1.607	-1.450	-0.720	-0.630	-0.107	0.107	0.630	0.720	1.450

The approximation to $f_R(R)$, the probability density function (pdf) of R, is given by the derivative of $S(R)$ which is just a function which is constant on each of the subintervals, $[R_i, R_{i+1}]$. From Table 5.1 and Figure 5.2, one can see that $S'(R)$ will be an even function, and this allows it to be simplified to

$$S'(R) = \sum_{i=1}^{5} c_i \Pi\left(\frac{R}{t_i}\right) \tag{5.2}$$

where c_i and t_i are functions of the R_i's and $\Pi(\cdot)$ is the rectangular pulse function which is defined as follows:

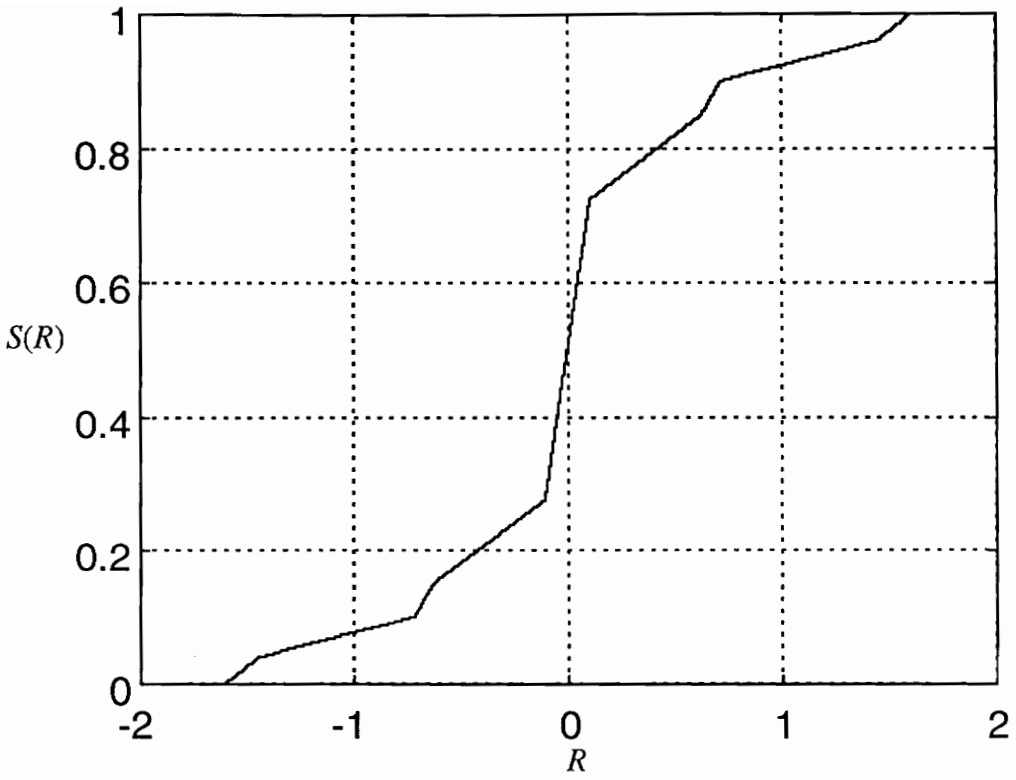

Figure 5.2 - Plot of the linear spline approximation to $F_R(R)$

$$\Pi\left(\frac{t}{T}\right)=\begin{cases}1, & |t|\le\frac{T}{2}\\ 0, & |t|>\frac{T}{2}\end{cases}. \tag{5.3}$$

The characteristic function of a random variable, given its pdf $f(x)$, is defined as [12]

$$\Phi(\omega)=\int_{-\infty}^{\infty} f(x)e^{j\omega x}dx=\mathfrak{F}\{f(-x)\} \tag{5.4}$$

where $\mathfrak{F}\{\cdot\}$ denotes the Fourier transform and $j=\sqrt{-1}$. Thus, using a table of Fourier transform pairs [17], the characteristic function of R can be approximated by

$$\Phi_R(\omega) \approx \sum_{i=1}^{5} c_i t_i \operatorname{sinc}\left(\frac{\omega t_i}{2\pi}\right) = \sum_{i=1}^{5} a_i \operatorname{sinc}\left(\frac{\omega t_i}{2\pi}\right) \tag{5.5}$$

where sinc(x) is defined as

$$\operatorname{sinc}(x) = \frac{\sin(\pi x)}{\pi x}. \tag{5.6}$$

Table 5.2 lists the values of a_i and t_i that correspond to the values of R_i given in Table 5.1.

Table 5.2 - Values used for a_i and t_i

i	1	2	3	4	5
a_i	0.399	-0.399	0.682	-0.502	0.820
t_i	0.213	1.260	1.440	2.900	3.213

5.4. Computing the Characteristic Function of the Total Receiver Noise

The random variable $n_i^{(k)}$ discussed back in Chapter 3 is related to the random variable R, and is given by

$$n_i^{(k)} = \begin{cases} \sqrt{P_k} E_w R, & \text{given a hit occurs} \\ 0, & \text{given no hit occurs} \end{cases}. \tag{5.7}$$

where the probability of a hit occurring, P_h, is given by (3.16). Thus, the characteristic function of $n_i^{(k)}$ is given by

$$\Phi_i^{(k)}(\omega) = P_h \Phi_R\left(E_w \sqrt{P_k}\omega\right) + 1 - P_h \tag{5.8}$$

using the following three facts [12]:

$$y = ax \Rightarrow \Phi_y(\omega) = \Phi_x(a\omega) \tag{5.9}$$

$$y = \begin{cases} x, & \text{given } A \\ z, & \text{given } B \end{cases} \Rightarrow \Phi_y(\omega) = P(A)\Phi_x(\omega) + P(B)\Phi_z(\omega) \tag{5.10}$$

$$y = 0 \Rightarrow f_y(y) = \delta(y) \Rightarrow \Phi_y(\omega) = 1. \tag{5.11}$$

Then, using (3.9), the characteristic function of the total receiver noise is given by

$$\Phi_T(\omega) = e^{-\frac{1}{2}\sigma_o^2\omega^2} \prod_{k=2}^{N_u} \left(P_h \Phi_R\left(E_w \sqrt{P_k}\omega\right) + 1 - P_h \right)^{N_b} \tag{5.12}$$

using (5.9) and the following fact [12]:

$$z = x + y \Rightarrow \Phi_z(\omega) = \Phi_x(\omega)\Phi_y(\omega). \tag{5.13}$$

The σ_o^2 in (5.12) is given by (3.11) which can be simplified as follows:

$$\sigma_o^2 = 0.225 \frac{P_1 N_b^2 \tau_m^2}{E_b/N_o}. \tag{5.14}$$

If the interfering users can be divided into N_g groups with U_i users in the i^{th} group where all users in the i^{th} group have relative power P_i, then (5.12) can be rewritten as

$$\Phi_T(\omega) = e^{-\frac{1}{2}\sigma_o^2\omega^2} \prod_{i=1}^{N_g} \left(P_h \Phi_R\left(E_w \sqrt{P_i}\omega\right) + 1 - P_h \right)^{N_b U_i}. \tag{5.15}$$

This simplification is the same as one used by Geraniotis [9], and it reduces the required computation time by reducing the number of factors in the product.

5.5. Computing the Probability of Error Using Characteristic Functions

The cdf of a random variable can be determined from its characteristic function by using the formula [18]

$$F(x) = \frac{1}{2} + \frac{1}{\pi} \int_0^\infty \frac{\mathrm{Re}\{\Phi(\omega)\}\sin(x\omega) + \mathrm{Im}\{\Phi(\omega)\}\cos(x\omega)}{\omega} d\omega \tag{5.16}$$

where $\mathrm{Re}\{\cdot\}$ and $\mathrm{Im}\{\cdot\}$ denote the real and imaginary parts of $\Phi(\omega)$, respectively. By looking back at (5.5) and (5.15), one can see that $\Phi_T(\omega)$ is a real function. This fact allows the cdf of the total receiver noise to be simplified to

$$F_T(x) = \frac{1}{2} + \frac{x}{\pi} \int_0^\infty \Phi_T(\omega) \mathrm{sinc}\left(\frac{\omega x}{\pi}\right) d\omega. \tag{5.17}$$

Finally, the probability of error can be computed by using

$$P_e = F_T(-m_0) = \frac{1}{2} - \frac{m_0}{\pi}\int_0^{\infty} \Phi_T(\omega)\,\mathrm{sinc}\left(\frac{\omega m_0}{\pi}\right) d\omega \tag{5.18}$$

where m_0 is given in (3.4), but can be simplified as follows:

$$m_0 = 0.6\sqrt{P_1}N_b\tau_m. \tag{5.19}$$

Thus, by using (5.18), one can compute P_e using a numerical integration. The only problem is that the upper limit of integration is infinity. This can be solved by truncating the numerical integration at some large, but finite upper limit. By inspecting (5.15), one can see that the integrand is guaranteed to approach zero as ω approaches infinity by the Gaussian factor which depends upon σ_o^2. Thus, one can use the value of σ_o^2 to determine an upper limit which will not introduce much error. In all the results which use this technique, the upper limit was set to $5/\sigma_o$ so that the integrand would be negligible for larger values of ω. To compute the integral, an 8192 point Simpson's Rule integration was used.

The steps involved in the overall computation are very simple. First, using the desired parameters, the values from Table 5.2, (5.15), and (5.18), the integrand of (5.18) is evaluated at 8192 points from 0 to $5/\sigma_o$. Then, Simpson's Rule is used to evaluate the integral. Finally, (5.18) is used with the value of the integral to calculate P_e.

5.6. Comparing the Numerical Analysis with the Simulation Results

Figure 5.3 shows the same simulation results that were shown in Figure 4.2 along with the corresponding numerical solutions. Because the Gaussian approximation did a good job of predicting performance for this value of N_b, Figure 5.3 does not look much different from Figure 4.2. However, by comparing the two figures, one can see that the numerical solutions are slightly better than the Gaussian approximation.

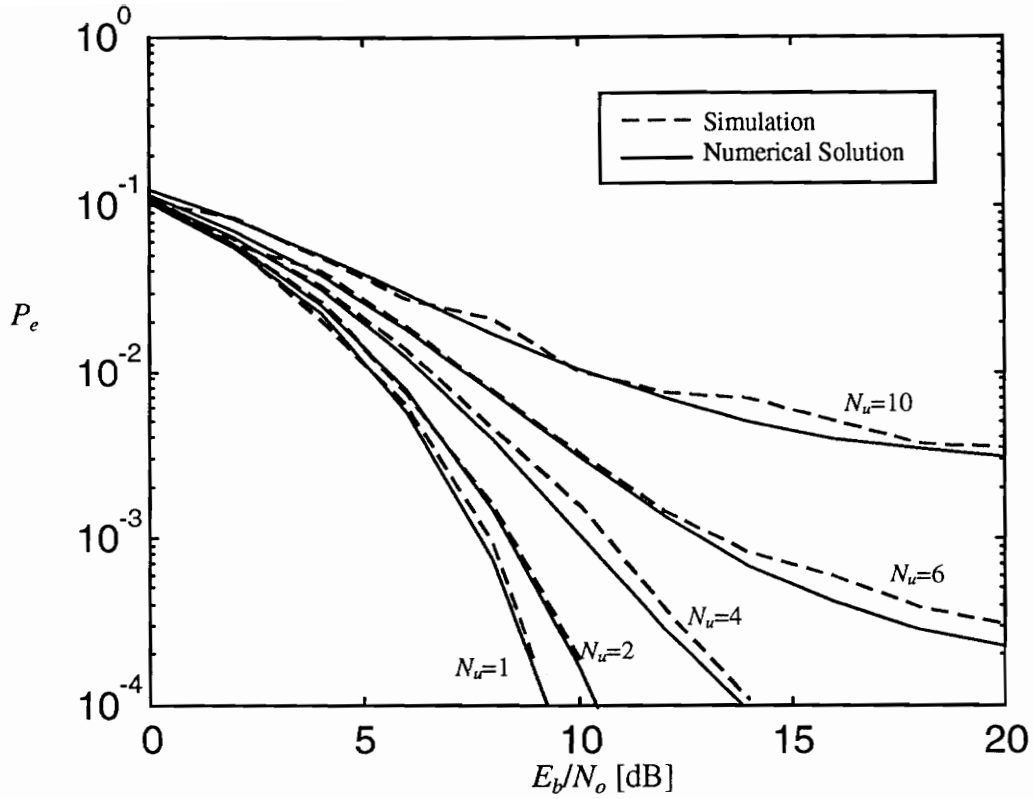

Figure 5.3 -Plot of P_e vs. E_b/N_o for different values of N_u with N_b=6 and T_f=80

Figures 5.4 and 5.5 shows the same simulation data as Figures 4.3 and 4.5 did with the corresponding numerical solutions. Here, one can see the improved accuracy of the numerical solution. As opposed to the Gaussian approximation, the numerical solution seems to correctly predict the dependence of the performance on N_b. The numerical solution seems to be consistently optimistic, and it becomes increasingly optimistic as N_b increases. However, on the whole, the numerical solution provides rather accurate results without the need for simulation.

Figures 5.6 and 5.7 are analogous to Figures 4.4 and 4.6 and show what happens for large values of N_b. As can be seen, the numerical solution does not do much better than the

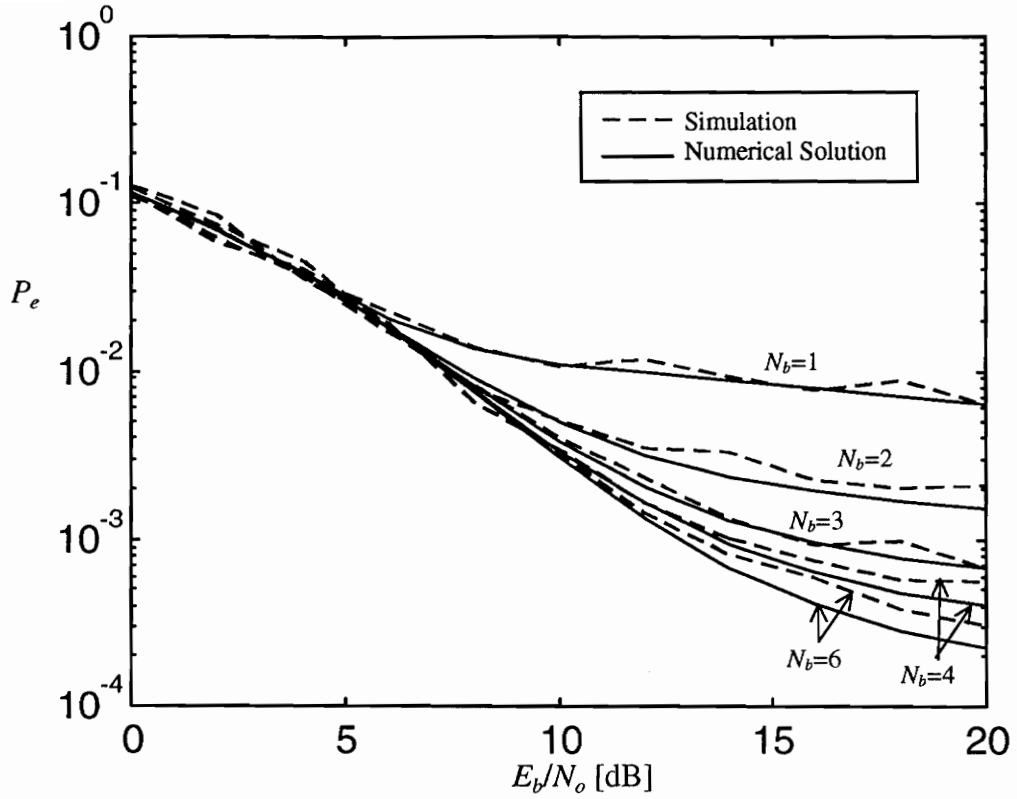

Figure 5.4 - Plot of P_e vs. E_b/N_o for different values of N_b with N_u=6 and N_bT_f=480

Gaussian approximation in predicting the simulation results. In fact, the numerical solution actually shows P_e decreasing for larger values of N_b. These poor results should not be too surprising since it was presumed in Chapter 4 that the drop in performance was due to dependence of the multiple access interference. Like the Gaussian approximation, the numerical solution assumes the $n_i^{(k)}$'s are independent. Thus, it seems that in order to correctly predict the performance for large values of N_b, a method which models the dependence of the multiple access interference must be used. However, these situations are of little practical importance since they correspond to small frame sizes, and would cause significant interference to existing narrowband systems.

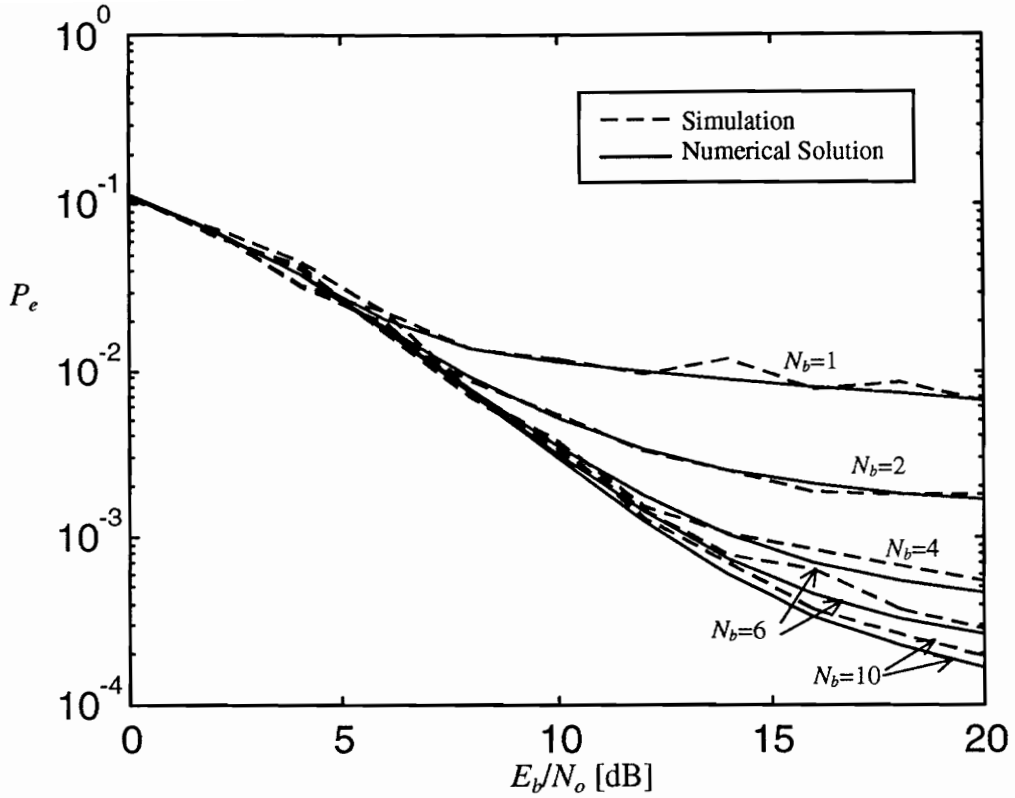

Figure 5.5 - Plot of P_e vs. E_b/N_o for different values of N_b with N_u=11 and N_bT_f=960

Looking back at Figures 5.4 and 5.5, it would seem that dependence between the $n_i^{(k)}$'s might also be what causes the numerical solution to become increasingly optimistic as N_b increases. This would also explain why the numerical solutions for the system with N_bT_f=960 are less optimistic than those for the system with N_bT_f=480. This is because the corresponding frame sizes are larger for this system, and thus, the dependence of the interference should be weaker.

Figure 5.8 shows the numerical results corresponding the results that were shown in Figure 4.7. Again, the numerical solution does a very good job of predicting the simulation results. Like the previous results, the performance predicted by the numerical

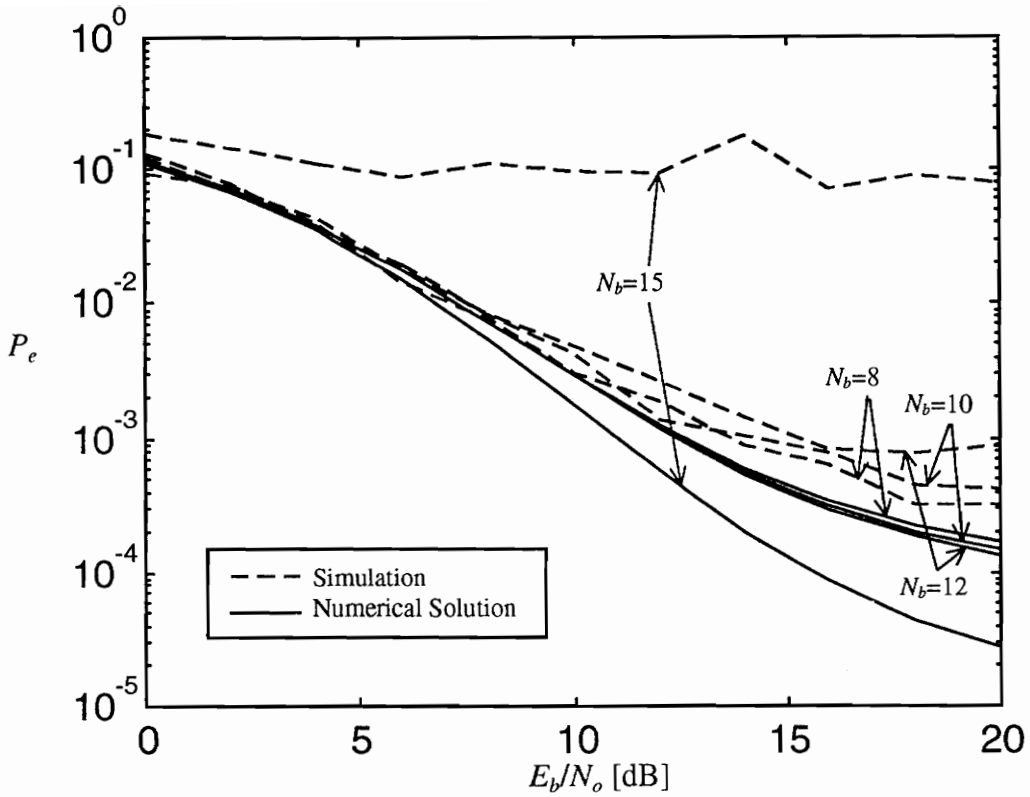

Figure 5.6 - Plot of P_e vs. E_b/N_o for different values of N_b with N_u=6 and N_bT_f=480

solution is slightly optimistic.

Figure 5.9 shows the effect of the interference power level as Figure 4.8 did. As was seen before, the numerical solution does a very good job of modeling the system for small and moderate values of N_b. Thus, it can completely predict the unusual performance seen in the simulation results.

5.7. Summary of Results

The results presented in this chapter show that the numerical analysis correctly predicts the performance of the UWB/TH system for a wide range of situations. The only

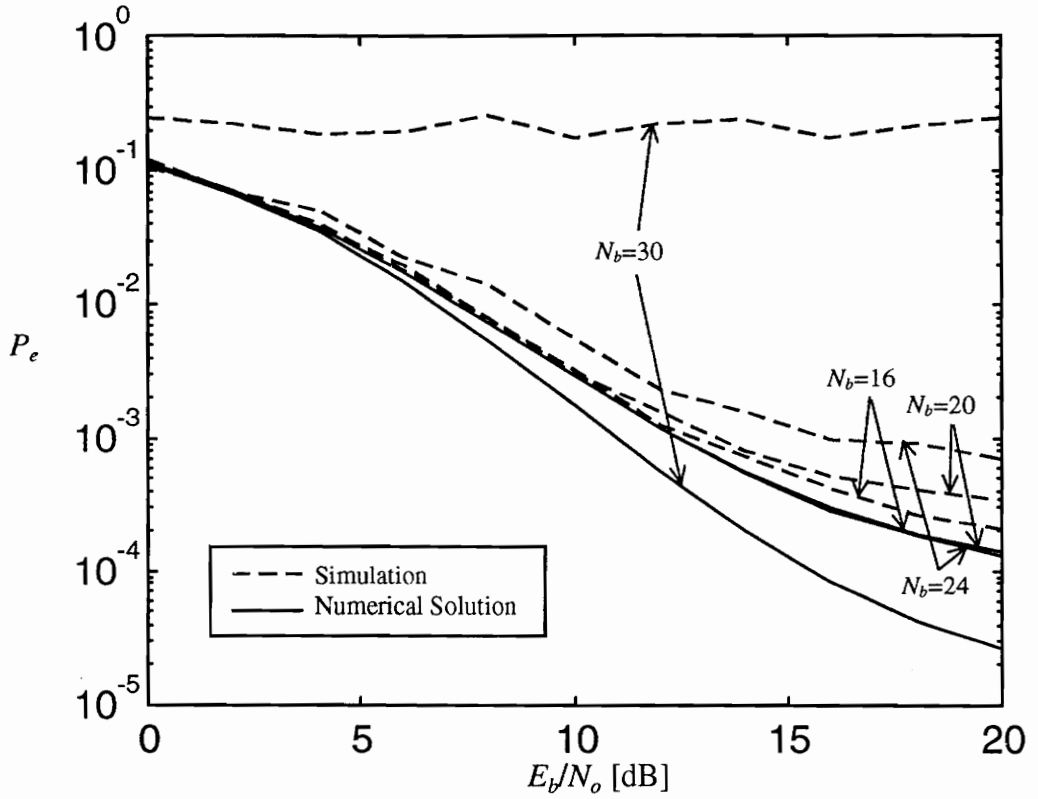

Figure 5.7 - Plot of P_e vs. E_b/N_o for different values of N_b with N_u=11 and N_bT_f=960

situations where the numerical analysis fails to predict the performance correctly are when the frame sizes are small and thus the dependence of the interference is significant. However, these situations are of little practical importance. This is because these situations represent systems which have almost no interference rejection capabilities and which would cause significant interference for existing narrowband users

The results from this chapter also contribute to the understanding of the system by confirming under what circumstances the Gaussian approximation fails and why it fails. The results show that the failure is not due to dependence of the interference because the numerical analysis correctly predicts performance while still assuming independence.

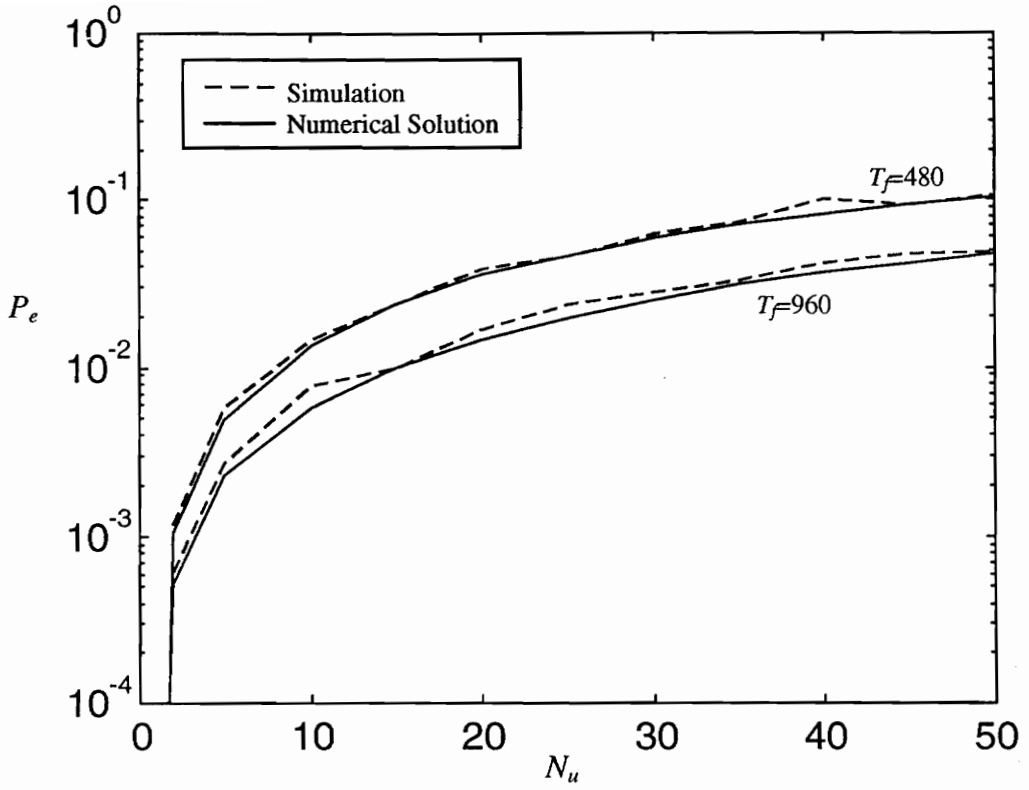

Figure 5.8 - Plot of P_e vs. N_u for different values of T_f with N_b=1 and E_b/N_o=20 dB

Results from Chapter 4 actually show that the Gaussian approximation holds as either N_u or N_b are increased. The problem is that the convergence rates for different situations vary, and in some situations, a large value of N_bN_u is needed for convergence. Results for Chapter 4 also seem to indicate that the convergence rate is affected by the value of T_f.

In the next chapter, the Gaussian approximation will be examined in more detail in order to explain why the convergence rate varies with T_f. This examination will help to provide intuitively satisfying explanations to most of the results seen in this thesis.

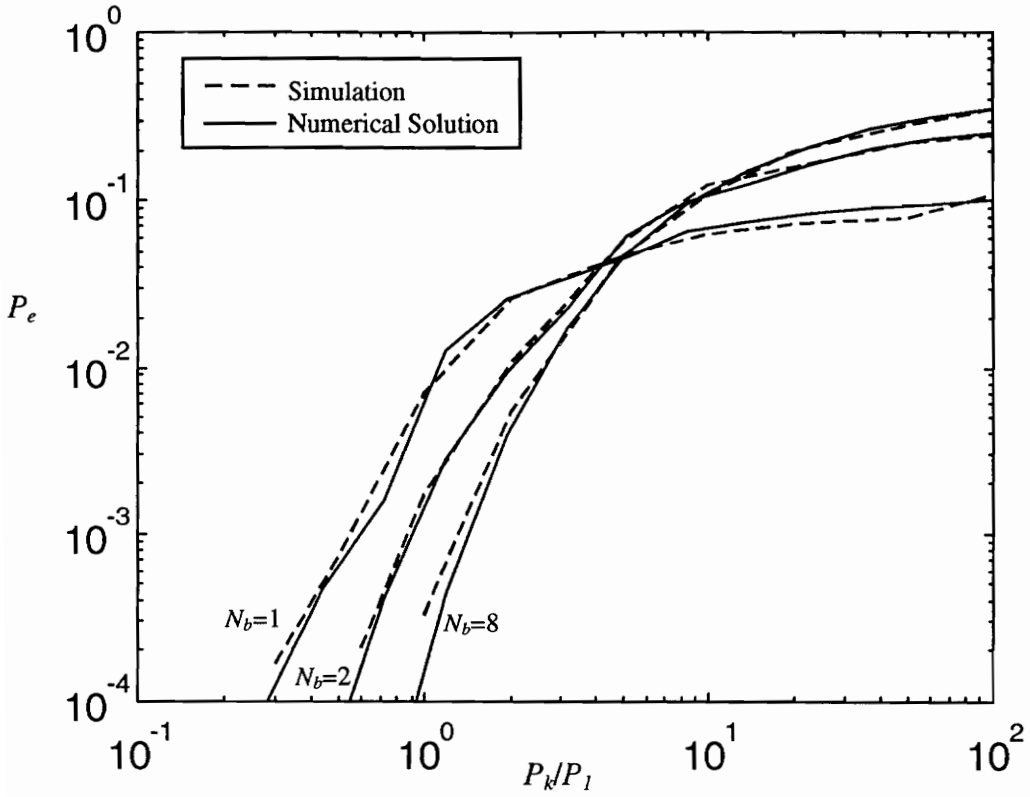

Figure 5.9 - Plot of P_e vs. P_k/P_1 for different values of N_b with N_u=6, N_bT_f=480, and E_b/N_o=20 dB

6. Discussion of Results

6.1. Insight Gained From the Numerical Analysis

The results from Chapter 5 show more than just an accurate method of analyzing the performance of the UWB time hopping system. They also help to answer the question of why the Gaussian approximation does not apply for small values of N_b. The only real difference between the Gaussian approximation and the numerical solution is that the numerical solution used an approximation to the distribution of the multiple access interference while the Gaussian approximation only used the variance. Both methods use the same general model for the interference and the same independence assumptions. This means that the Gaussian approximation is not failing because of dependence of the interference as is the case for DS/SS systems. Thus, there must be something about the total distribution of the multiple access interference which causes the convergence properties to change in different situations. Previous results have indicated that convergence occurs as either N_u or N_b are increased but is affected by the value of T_f.

6.2. A Look at the Convergence of the Gaussian Approximation

The second characteristic function is defined as [12]

$$\Psi(\omega) = \ln \Phi(\omega). \tag{6.1}$$

Using a Taylor Series expansion, $\Psi(\omega)$ can be written as [18]

$$\Psi(\omega) = \sum_{n=1}^{\infty} \kappa_n \frac{(j\omega)^n}{n!} \tag{6.2}$$

where the κ_n's are called the cumulants of the distribution and are related the distribution's moments. For a standard normal distribution, $\Psi(\omega)$ is given by

$$\Psi(\omega) = \frac{-\omega^2}{2}. \tag{6.3}$$

Thus, if it can be shown that a particular $\Psi(\omega)$ converges to (6.3), then the corresponding distribution will converge to a standard normal distribution. In fact, this method is used quite often in proofs of the CLT [19].

In order to examine the convergence of the Gaussian approximation, the second characteristic function of n_I, the noise due to multiple access interference, will be used. However, in order to use the strategy outlined above, n_I must be normalized so that it will converge to a standard normal distribution. This normalized random variable, I is given by

$$I = \frac{n_I}{\sigma} \tag{6.4}$$

where σ is the standard deviation of n_I. Using (3.13) and (5.7), one can show that σ is given by

$$\sigma = E_w \sqrt{P_h N_b m_2^{(R)} \sum_{k=2}^{N_u} P_k} \tag{6.5}$$

where $m_2^{(R)}$ is the second moment of the random variable R which was discussed back in Chapter 5. It was shown in (5.13) that the characteristic function of the sum of random variables is the product of their individual characteristic functions. Thus, the second characteristic function of a sum is just the sum of the individual second characteristic functions. Using this fact and (6.4) allows the second characteristic function of I to be given by

$$\Psi_I(\omega) = \sum_{n=1}^{\infty} \frac{1}{n!} \left(\frac{j\omega}{\sigma} \right)^n \sum_{k=2}^{N_u} \sum_{i=0}^{N_b-1} \kappa_n^{(i,k)} \tag{6.6}$$

where $\kappa_n^{(i,k)}$ is the n^{th} cumulant of $n_i^{(k)}$. Because $n_i^{(k)}$ is a zero mean random variable, the relationships between its first several cumulants and its moments are given by [18]

$$\kappa_1^{(i,k)} = 0 \tag{6.7}$$

$$\kappa_2^{(i,k)} = m_2^{(i,k)} \tag{6.8}$$

$$\kappa_3^{(i,k)} = m_3^{(i,k)} \tag{6.9}$$

$$\kappa_4^{(i,k)} = m_4^{(i,k)} - 3\left(m_2^{(i,k)}\right)^2 \tag{6.10}$$

$$\kappa_5^{(i,k)} = m_5^{(i,k)} - 10 m_3^{(i,k)} m_2^{(i,k)} \tag{6.11}$$

$$\kappa_6^{(i,k)} = m_6^{(i,k)} - 15m_4^{(i,k)}m_2^{(i,k)} - 10\left(m_3^{(i,k)}\right)^2 + 30\left(m_2^{(i,k)}\right)^3 \tag{6.12}$$

where $m_n^{(i,k)}$ denotes the n^{th} moment of $n_i^{(k)}$. By using (5.7) one can easily determine that the moments of $n_i^{(k)}$ are given by [12]

$$m_n^{(i,k)} = P_h\left(E_w\sqrt{P_k}\right)^n m_n^{(R)}, \text{ for } n = 1,\ 2,\ \ldots \tag{6.13}$$

where $m_n^{(R)}$ is the n^{th} moment of R. Looking back at Chapter 5, one can see that because the distribution of R is symmetric, the odd moments of R will be zero. Thus, by putting everything together, the Taylor Series expansion of the second characteristic function of I is given by

$$\Psi_I(\omega) = -\frac{\omega^2}{2} + \frac{\omega^4}{24}\frac{1}{N_b}\frac{\sum_{k=2}^{N_u} P_k^2}{\left(\sum_{k=2}^{N_u} P_k\right)^2}\left[\frac{1}{P_h}\frac{m_4^{(R)}}{\left(m_2^{(R)}\right)^2} - 3\right]$$

$$-\frac{\omega^6}{720}\frac{1}{N_b^2}\frac{\sum_{k=2}^{N_u} P_k^3}{\left(\sum_{k=2}^{N_u} P_k\right)^3}\left[\frac{1}{P_h^2}\frac{m_6^{(R)}}{\left(m_2^{(R)}\right)^3} - \frac{15}{P_h}\frac{m_4^{(R)}}{\left(m_2^{(R)}\right)^2} - 30\right] + \sum_{n=4}^{\infty}\kappa_{2n}^I\frac{(j\omega)^{2n}}{(2n)!} \tag{6.14}$$

where κ_{2n}^I is the $2n^{th}$ cumulant of I. If all the P_k's are equal and if (3.16) is used, then (6.14) can be simplified to

$$\Psi_I(\omega) = -\frac{\omega^2}{2} + \frac{\omega^4}{24}\frac{1}{N_b(N_u - 1)}\left[\frac{T_f}{4\tau_m}\frac{m_4^{(R)}}{\left(m_2^{(R)}\right)^2} - 3\right]$$

$$-\frac{\omega^6}{720}\frac{1}{N_b^2(N_u - 1)^2}\left[\frac{T_f^2}{16\tau_m^2}\frac{m_6^{(R)}}{\left(m_2^{(R)}\right)^3} - \frac{15T_f}{4\tau_m}\frac{m_4^{(R)}}{\left(m_2^{(R)}\right)^2} - 30\right] + \sum_{n=4}^{\infty}\kappa_{2n}^I\frac{(j\omega)^{2n}}{(2n)!}. \tag{6.15}$$

Equation (6.15) provides much insight into the conditions under which the Gaussian approximation applies. Equation (6.15) shows that when either N_b or N_u become large, all the terms except the ω^2 term will vanish, and thus, the distribution will converge to a

standard normal distribution. Hence, with N_b and T_f fixed, the multiple access interference will converge to Gaussian noise as N_u is increased. This phenomenon was seen before in the previous results, and it is shown again in Figure 6.1. Figure 6.1 is a plot of P_e vs. N_u for different values of T_f with N_b=1 and E_b/N_o=20 dB, and it compares the Gaussian approximation to the numerical solution. The plot definitely shows that the Gaussian approximation predicts performance better as the number of users increases. From Figure 6.1, one can also see that the number of users needed for convergence seems to be linearly dependent on T_f. Equation (6.15) also predicts that when N_u and T_f are fixed, the multiple access interference will converge to Gaussian noise as N_b is increased. This effect is seen in Figure 6.2 which is a plot of P_e vs. N_b for different values of T_f with N_u=15 and E_b/N_o=12 dB. Interestingly, this plot shows that the convergence rate in this situation is

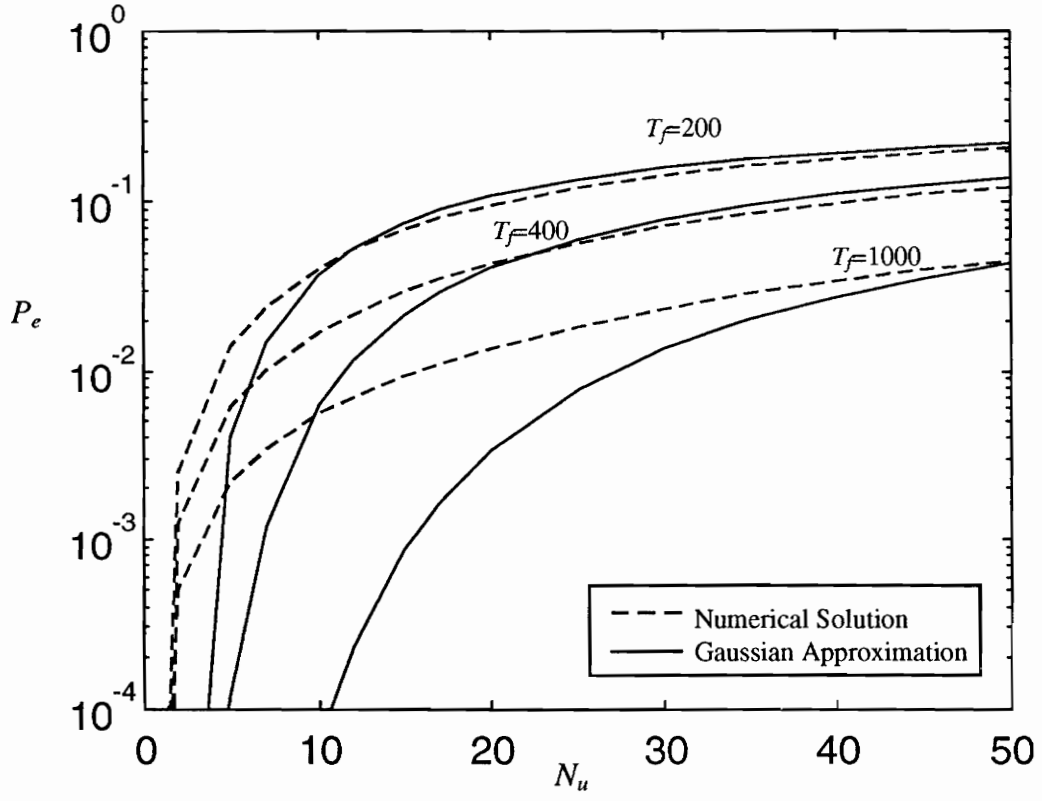

Figure 6.1 - Plot of P_e vs. N_u for different values of T_f with N_b=1 and E_b/N_o=20 dB

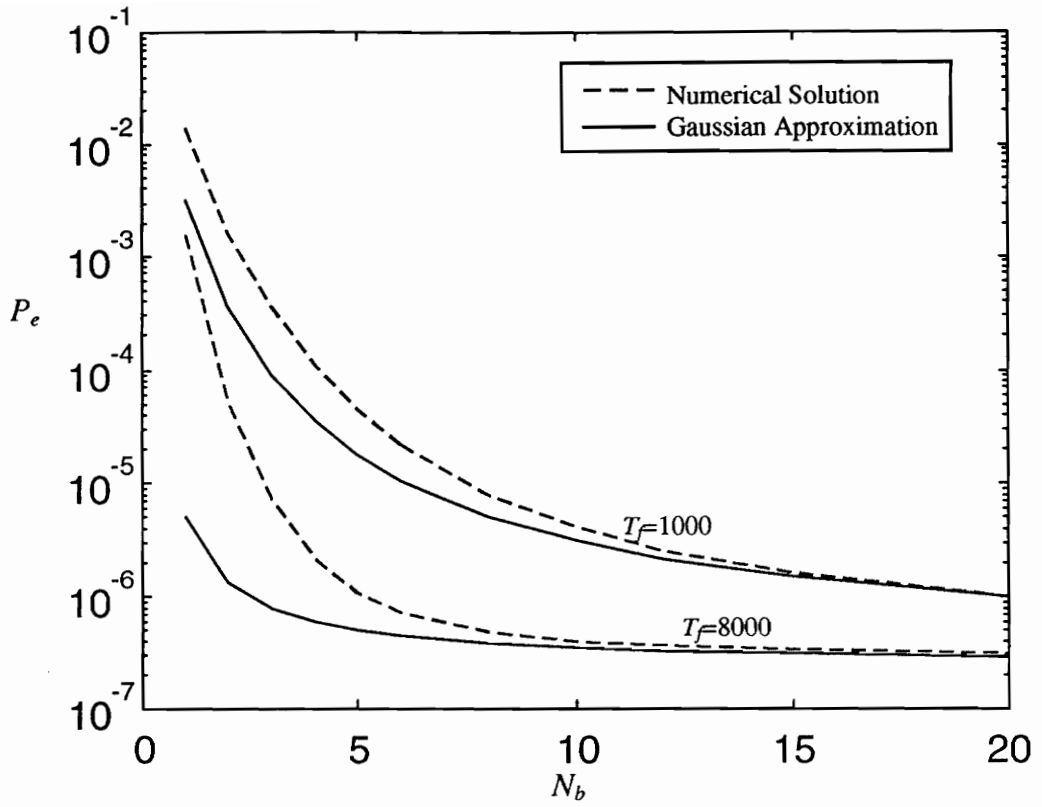

Figure 6.2 - Plot of P_e vs. N_b for different values of T_f with N_u=15 and E_b/N_o=12 dB

only slightly dependent on T_f. Some of the earlier results also showed that the Gaussian approximation becomes more accurate as N_b increases, but these situations were for a fixed N_bT_f. This type of convergence is shown in Figure 6.3 which is a plot of P_e vs. N_b for different values of N_bT_f with N_u=15 and E_b/N_o=20 dB. This plot also shows that the convergence rate for this situation is approximately linearly dependent on T_f. Both this plot and (6.15) do not predict that the Gaussian approximation will again become optimistic as N_b becomes large, but this is because the numerical solution and (6.15) assume that the $n_i^{(k)}$'s are independent.

From (6.15), it is easy to see how T_f can affect the convergence. Each higher order term

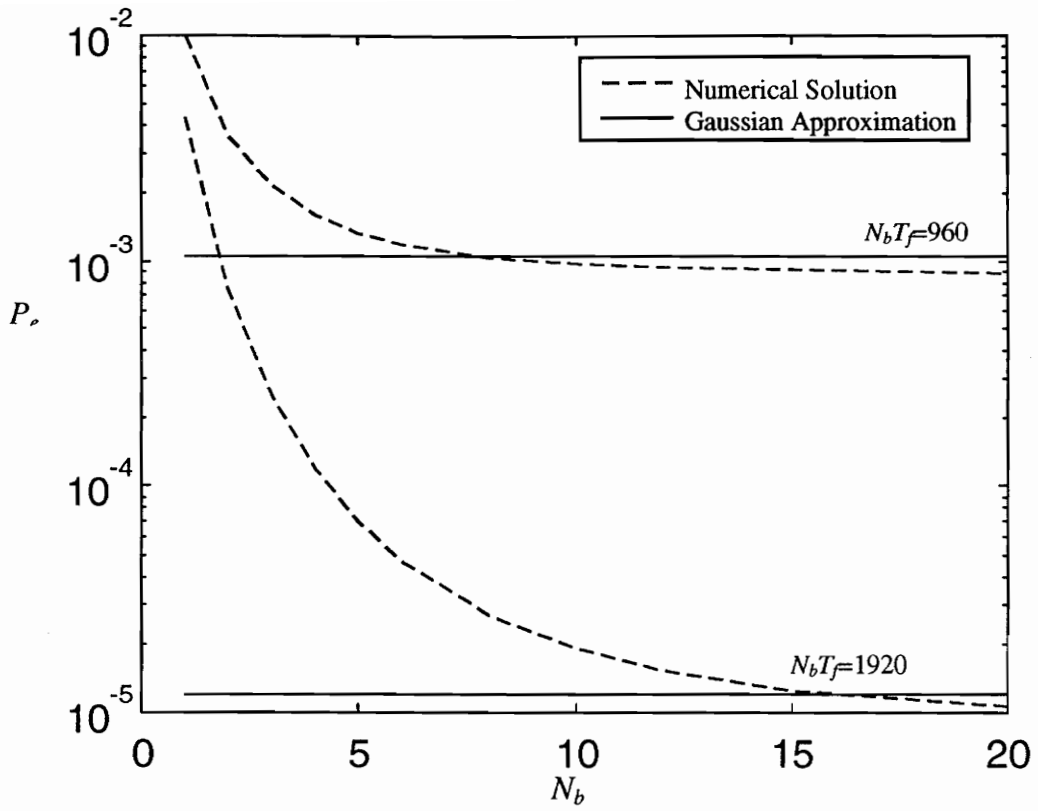

Figure 6.3 - Plot of P_e vs. N_b for different values of N_bT_f with N_u=15 and E_b/N_o=20 dB

in (6.15) increases as T_f increases, and thus, a large value of T_f can slow the convergence so that much larger values of N_u or N_b are needed. By looking back at (6.14) and (6.15), one can see that for moderately large values of T_f (and thus moderately small values of P_h), the higher order terms are roughly proportional to powers of $1/N_bN_uP_h$. Thus, convergence is guaranteed if the product $N_bN_uP_h$ is large. This way of looking at the problem is very intuitively satisfying because the product $N_bN_uP_h$ is equal to the average number of hits per bit assuming that the hits are independent. Thus, as long as there are a moderate number of hits per bit, then the combination of those hits will appear like Gaussian noise. This shows that the assumption that the number of $n_i^{(k)}$'s governs the convergence of the Gaussian approximation was wrong. However, in hindsight, this

makes sense, for if a hit does not occur, then the corresponding $n_i^{(k)}$ does not contribute any interference. This means that the product $N_b N_u P_h$ also represents the average number of non-trivial random variables which contribute to the interference and is thus a better indicator of convergence. However, the product $N_b N_u P_h$ gives only a rough estimate of the convergence properties. This is seen in Figure 6.2 where the convergence is shown to be relatively independent of T_f which is not what the factor $N_b N_u P_h$ would predict. The situations seen in Figures 6.1 and 6.3, however, show convergence rates which are proportional to $N_b N_u P_h$.

The product $N_b N_u P_h$ shows that even though a system might have a low probability of a hit, P_h, the performance could still be poor if the probability of an error given a hit occurred, $P_{e|h}$, is large. This is exactly the problem with the time hopping system, for when T_f is increased, the degradation due to the increase in $P_{e|h}$ outweighs the improvement due to the decrease in P_h. Thus, "smoothing" the distribution of the interference has a bigger impact on performance than does reducing the number of hits.

Thinking in terms of P_h and $P_{e|h}$ also helps to explain the results seen in Figure 5.9. There it was shown that using N_b=1 gave better performance when the multiple access interference had a large power level, and larger values of N_b gave better performance when the power of the multiple access interference was small. When the power of the multiple access interference becomes large, $P_{e|h}$ becomes large enough so that better performance is achieved by making P_h as small as possible. For a fixed processing gain, this means choosing N_b to be 1. For moderate and small power levels, however, it is more effective to reduce $P_{e|h}$, which means increasing N_b.

As can be seen, looking at the system in terms of P_h and $P_{e|h}$ provides much insight into its performance. This is similar to the way that frequency hopped systems are usually analyzed. However, by this point it should be rather apparent that the time hopping

system has much more in common with a frequency hopping system than with a direct sequence system. This is probably a reason why the Gaussian approximation does not predict some of the interesting behavior seen before. The performance of the time hopping system in circumstances where P_h is small and $P_{e|h}$ is large also resembles the performance of a frequency hopping system. This suggests the need for error correction coding in these circumstances as is commonly used with frequency hopping.

One final and interesting point that can be made with the help of (6.15) is that the dependence of the performance on N_b and T_f is strictly due to the time hopping multiple access technique used. Even though a change in the pulse shape or in the modulation format would affect the distribution of the interference, they will not change how N_b and T_f affect performance. These effects are related to the average number of hits per bit and not to the type of interference which each hit causes.

6.3. Significance of Important Performance Results

In addition to examining the Gaussian approximation and presenting a more accurate analysis, this thesis has also shown some significant performance results that were not predicted by the Gaussian approximation. One of these results was shown in Figure 5.9. Here it was show that the power level of the multiple access interference determined what values of N_b gave better performance. The power levels of other users will probably not fluctuate over the large range shown in the plot, especially if power control is used. However, these results are important because they show what will happen when the channel has multipath components. The short monocycle width causes all but very short path differences to be treated as if they were multiple access interference from other users. This will slightly raise the total interference level, but more importantly, it will "steal" power away from the desired user's signal. Thus, unless a RAKE receiver is used, the ratio of the other user's power level to the desired user's power level could become rather large. If this ratio becomes large enough, then as Figure 5.9 shows, reducing P_h will

improve performance more than reducing $P_{e|h}$.

The most important performance result shown earlier is that the performance of the time hopping system can be poor when N_b is small. However, how this result effects system design depends on what parameters are fixed and what parameters can be varied. Up until now, it was assumed that the processing gain, $N_b T_f / T_m$, was fixed. This is true for other spread spectrum systems since the required bandwidth must be kept as small as possible. This means choosing the smallest processing gain which will still provide the necessary performance. For a time hopping system, this will not necessarily be the case. One of the major concerns for this system is keeping the duty cycle low and the bandwidth large so that the system does not significantly interfere with narrowband systems. For systems which also need location information, the pulse width should be small. All of these requirements mean that T_m should be small and T_f should be large. Both of these conditions are limited by the accuracy and stability of the clocks used in the system [3]. Thus, these two parameters are normally fixed to whatever values are currently achievable. Systems that are currently being developed have T_m's on the order of a nanosecond and T_f's about 100 to 1000 times T_m.

With a fixed T_f, the value of N_b will be solely determined by the required data rate of the source, and the maximum data rate possible would just be equal to $1/T_f$. For the values of T_m and T_f mentioned above, this means that unless the data rate is very large, the value of N_b will be relatively large. How good the performance will be will depend on N_u. Not only will the value of N_u be limited because it will degrade the system performance, but there is again the more restrictive constraint that the system should not interfere with other systems. The interference level this system causes will be proportional to N_u, and this constraint will keep N_u from becoming large even if the system performance would not degrade much. All this means that unless the value of N_b is extremely large, the product $N_b N_u P_h$ will be small. Thus, unless the data rate of the source is very small, the

performance of the system will be limited by a large $P_{e|h}$.

The fact that the system will be operating with a large $P_{e|h}$ most of the time suggests the need for error correction coding. In fact the system discussed so far can actually be viewed as a coded system. The code in this case is just a simple repetition code. This suggests that a more sophisticated code could be used in place of this simple code. Thus, the system could use any (n,k) code where n would be equal to N_b. The only issue that must be kept in mind is that the source data rate and the code rate will be limited because the fixed T_f puts a hard upper limit on the symbol rate which can be transmitted.

7. Conclusion

7.1. Summary of Thesis Results

First, a simulation of the UWB PPM time hopping system was presented in order to test the standard Gaussian approximation. The results of this simulation showed a few situations in which the Gaussian approximation failed to accurately predict performance. When N_b is large, the performance is worse than the Gaussian approximation because of bit error dependencies, but this situation does not represent a practical system. More importantly, the performance again is worse than the Gaussian approximation when N_b is small. Another interesting result is that for smaller values of N_b the performance is better than the Gaussian approximation when the other user's power is large but worse when the other user's power is small.

In order to try to duplicate these simulation results, a numerical analysis which modeled the complete distribution of the interference was used. The results of this analysis showed that most of the effects seen in the simulation results are correctly predicted by the numerical analysis. The only exception is when there is significant bit error dependence. This is because the numerical analysis assumed that all hits are independent of each other. Because this analysis predicts the performance rather well, it may aid in the design and analysis of future UWB time hopping communication systems.

Insight gained from the numerical analysis prompted an analysis of the convergence of the Gaussian approximation. This explained why the Gaussian approximation failed under certain circumstances. It also showed that the time hopping system should really be analyzed using a method similar to that used for frequency hopping. Then, the implications of some of the earlier performance results were discussed. It was mentioned that the results of the effect of the other's users power level could help to determine the effects of a multipath channel. The implications of the effect of N_b on performance were also discussed, and it was pointed out that error correction coding could help to provide

better performance

7.2. Future Work

One area that needs to be studied is how error correction coding will affect the performance of the time hopping system. As mentioned in the last section, error correction coding could help to improve the performance when N_b is small. Also, it would be interesting to see how the performance is affected when the original repetition code is replaced by a more complex code with the same rate.

Examining the effects of more complicated channel models is also an area to be studied. However, as mentioned before, there are indications that multipath and Doppler channels will not have a severe effect on performance. The addition of narrowband interference to the channel model would help to show what effect this type of interference would have on performance. Rejecting narrowband interference is very important since it is likely that this type of interference will be at a much higher power level than the UWB signals.

8. References

[1] Paul Withington II and Larry W. Fullerton, "An Impulse Radio Communications System," *Ultra-Wideband Short Pulse Electromagnetics*, Henry L. Bertoni, Lawrence Carin, and Leopold B. Felsen eds., New York: Plenum Press, 1993.

[2] "Micropower Impulse Radar (MIR) Technology Overview," Lawrence Livermore National Laboratory, Livermore, CA, 1995.

[3] R. A. Scholtz, "Multiple Access with Time-Hopping Impulse Modulation," *MILCOM '93 Conference Record*, Bedford, MA, Oct. 11-14, 1993, pp. 447-450.

[4] R. A. Scholtz, "Multiple Access Capacity Estimate for Pulson's Digital Impulse Communication System," Report for Time Domain Systems, Inc., Huntsville, AL, 1993.

[5] Robert D. James and Jeffrey B. Mendola, "Ultra-wideband Communications Technology Applications in Intelligent Transportation Systems," To be published in the Proceedings of the 1996 ITS America Annual Meeting.

[6] Frank Wright, FCC, Personal Correspondence, August 1995.

[7] Alex W. Lam and Dilip V. Sarwate, "Time-Hopping and Frequency-Hopping Multiple-Access Packet Communications," *IEEE Transactions on Communications*, vol. 38, pp. 875-888, June 1990.

[8] Jiangzhou Wang and Marc Moeneclaey, "Multiple Hops/Symbol FFH-SSMA with MFSK Modulation and Reed-Solomon Coding for Indoor Radio," *IEEE Transactions on Communications*, vol. 41, pp. 793-801, May 1993.

[9] Evaggelos Geraniotis, "Multiple-Access Capability of Frequency-Hopped Spread-Spectrum Revisited: An Analysis of the Effect of Unequal Power Levels," *IEEE Transactions on Communications*, vol. 38, pp. 1066-1077, July 1990.

[10] M. B. Pursley, "Performance evaluation for phase-coded spread-spectrum multiple-access communication - Part I: system analysis," *IEEE Transactions on Communications*, vol. COM-25, pp.795-799, Aug. 1977.

[11] Larry Fullerton and Charles Carter, "Doppler Shift in Monocycle Communications," Report for Time Domain Systems, Inc., Huntsville, AL.

[12] Athanasios Papoulis, *Probability, Random Variables, and Stochastic Processes*, 3rd ed., New York: McGraw-Hill, Inc., 1991

[13] Robert K. Morrow, Jr. and James S. Lehnert, "Bit-to-Bit Error Dependence in Slotted DS/SSMA Packet Systems with Random Signature Sequences," *IEEE Transactions on Communications*, vol. 37, pp. 1052-1061, Oct. 1989.

[14] Jack M. Holtzman, "A Simple, Accurate Method to Calculate Spread-Spectrum Multiple-Access Error Probabilities," *IEEE Transactions on Communications*, vol. 40, pp. 461-464, March 1992.

[15] Michel C. Jeruchim, Philip Balaban, and K. Sam Shanmugan, *Simulation of Communication Systems*, New York: Plenum Press, 1992.

[16] Lars Eldén and Linde Wittmeyer-Koch, *Numerical Analysis: An Introduction*, Boston: Academic Press, Inc., 1990.

[17] Samir S. Soliman and Mandyam D. Srinath, *Continuous and Discrete Signals and Systems*, Englewood Cliffs: Prentice-Hall, Inc., 1990.

[18] Maurice G. Kendall, *Kendall's Advanced Theory of Statistics, Volume 1: Distribution Theory*, 6th ed., Alan Stuart and J. Keith Ord eds., New York: Halstead Press, 1994.

[19] M. Loève, *Probability Theory I*, 4th ed., New York: Springer-Verlag, 1977.

Vita

Jeffrey B. Mendola was born on December 13, 1971. He received his Bachelor of Science degree in Electrical Engineering from Pennsylvania State University in May 1990. In 1995, he joined the Center for Transportation Research at Virginia Polytechnic Institute and State University. His research there focused on sensors and communication systems for Intelligent Transportation Systems.